BOTSWANA INTERNATIONAL UNIVERSITY OF SCIENCE & TECHNOLOGY

School of Earth Sciences and Engineering

Department of Chemical, Material and Metallurgical Engineering

DEVELOPMENT OF MEMBRANES FROM COAL-DERIVED GRAPHENE OXIDE FOR ORGANIC DYE REMOVAL IN WASTEWATER TREATMENT

by

BOITSHEPHO IVY MARAKALALA

Student ID number: 22017768

BEng Hons (Metallurgical) (UJ)

A Thesis Submitted to the School of Earth Science and Engineering in Partial Fulfilment of the Requirements for the Award of the Degree of Master of Engineering in Chemical Engineering of BIUST

Supervisor(s):

Dr. Vepika Kandjou

Department of Chemical, Materials and Metallurgical Engineering

School of Earth Sciences and Engineering, BIUST

E-mail Address: kandjouv@biust.ac.bw

Prof. Freeman Ntuli

Department of Chemical, Materials and Metallurgical Engineering

School of Earth Sciences and Engineering, BIUST

E-mail Address: ntulif@biust.ac.bw

August, 2025

BOTSWANA INTERNATIONAL UNIVERSITY OF SCIENCE & TECHNOLOGY

POSTGRADUATE SCHOOL

Declaration Regarding the Work and Copyright

DECLARATION REGARDING THE WORK AND COPYRIGHT

Candidate : BOITSHEPHO IVY MARAKALALA

Student ID: 22017768

Thesis Titled: **DEVELOPMENT OF MEMBRANES FROM COAL-DERIVED GRAPHENE OXIDE FOR ORGANIC DYE REMOVAL IN WASTEWATER TREATMENT**

I, the **Candidate**, certify that the Thesis is all my own original work and that I have not obtained a degree in this University or elsewhere on the basis of any of this work.

(If the thesis is based on a group project, then the student must indicate the extent of her / his contribution, with reference to any other theses submitted or published by each collaborator in the project, and a declaration to this effect must be included in the thesis)

Signed:  Date: 26 August 2025

Primary Supervisor (please write in caps or type)

_____

I, the Candidate's **Primary Supervisor**, hereby confirm that I have inspected the above titled thesis and, to the best of my knowledge, it is based on the original work of the candidate.

Signed:  Date: 26/8/2025

Publications

Marakalala, B.I., Manisa, V.K., Lekgoba, T., Ntuli, F. and Kandjou, V., Coal to graphene based materials: Evaluating coal as a potential feedstock to pave way for large scale production of graphene and related materials, a review, Next Materials, Volume 7, 2025, 100519, ISSN 2949-8228, https://doi.org/10.1016/j.nxmate.2025.100519. (https://www.sciencedirect.com/science/article/pii/S2949822825000371

Marakalala, B.I., Nheta, W. and Baloyi, N.P., Structural Evolution of Coal Fines to Graphite Produced by Metal-Assisted Microwave Method. 39th JOHANNESBURG International Conferenceon "Chemical, Biological and Environmental Engineering"(JCBEE-23)Nov.16-17,2023 Johannesburg (South Africa), https://doi.org/10.17758/IICBE5.C1123039

Marakalala, B.I., Kandjou, V., Lekgoba, T. & Ntuli, F., 2025. The valorisation of coal fines to develop graphene oxide for effective utilisation in wastewater treatment through organic dye removal from contaminated waters. *Unpublished manuscript*, Materials Science & Engineering B, Manuscript no. MSB-D-25-01472.

Acknowledgements

I would like to extend my sincere gratitude to, Dr. V. Kandjou, and my co-supervisor, Prof. F. Ntuli, for their unwavering support, and guidance, during the duration of this project. Their guidance was essential to this work's effective completion. Additionally, I want to thank the Analytical and Mineral Processing Laboratory team for their invaluable assistance, with special thanks to Mr. T. Lekgoba and Prof. E. Malenga for their support during the experimental phases.

Abstract

Coal, though abundant, faces increasing restrictions due to its environmental impact as a fossil fuel. However, its carbon-rich nature presents opportunities for sustainable valorisation. This study explores the transformation of Botswana's coal fines, an underutilized waste product, into valuable carbon nanomaterials, specifically graphite and graphene oxide (GO). Graphitization of coal fines was followed by GO synthesis using an optimized version of the improved Hummers' method, producing highly hydrophilic GO with an oxygen content of up to 40.7 %. Comprehensive characterization techniques, including FTIR, Raman spectroscopy, and SEM-EDX, confirmed the compositional and morphological integrity of the graphite and GO. The synthesized GO was then used to fabricate membranes via a dead-end filtration method, with varying GO concentrations. These membranes demonstrated exceptional performance in removing Methylene Blue dye, achieving up to 99.8 % rejection, porosity of 13.2 %, and flux ranging from 0.62 to 17 L/m^2.hr. Additionally, a fouling resistance of 0.087 m^2.hr.bar/L indicated strong potential for long-term application. The findings highlight a cost-effective, environmentally friendly pathway for converting coal waste into purposeful GO membranes, designed for advanced water purification applications through selective dye removal mechanisms such as π-π interactions.

Keywords: Coal graphitisation, graphene oxide, Hummers' method, water treatment

Table of Contents

List of Tables

List of Figures

1 Chapter 1: INTRODUCTION

1.1 Background

Morupule coal mine produces 2.8 billion tons of coal annually, resulting in a significant amount of non-economic coal fines that are discarded and stockpiled (Medupe et al. 2019). These coal fines can be utilised for the production of crystalline graphite that can serve as a starting material for the production of Graphene Oxide (GO) (Manoj 2020; Singh, Haskin & Dastgheib 2023). Graphite is not only a GO precursor but a versatile material with various applications including pencil manufacturing, lubrication, refractories, lithium-ion batteries and control rods in nuclear reactors (Mukhopadhyay & Gupta 2012).

GO is a monolayer oxidised graphene which is relatively easy and cost-effective to produce in comparison to graphene (Marcano et al. 2018). As a result of its properties such as, aqueous processability, surface functionalisation ability, amphiphilicity, fluorescence and electrochemiluminescence, it is applicable in numerous industrial processes and technologies (Banerjee 2018). Depending on its oxidation degree, it can be used as a nanofiller to enhance thermal conductivity (when reduced), optical transparency, and mechanical and electrical properties aiding in the development of transparent and flexible conductors, fluorescence quenchers and Light Emitting Diodes (Plachá & Jampilek 2019; Rajakumar et al., 2020; Tamuly, Bhattacharjya & Saikia 2022). In water purification, treatment and desalination, GO is applicable as it has good hydrophilicity, a large aspect ratio and viable mechanical stability (Liu 2017). It can effectively remove toxic/hazardous contaminants that cannot be removed by conventional treatment technologies or methods (Ali et al. 2019). For instance, scientists at the Haldia Institute of Technology in India have developed a gravity filter using GO for purifying river water (Mukhopadhyay & Gupta 2012).

There are currently four significant GO synthesis methods: Brodie, Staudenmaier, Hofmann, and Hummers, each employing different oxidation strategies to convert graphite (Sun 2019). The Hummers method remains the most widely adopted approach because it is relatively safe and its scalability, it is predominantly used or slightly altered to generate GO (Smith et al. 2019). The efficiency of the oxidation process is typically assessed through the carbon to oxygen C/O ratio of the resulting GO material (Shi et al. 2021).

1.2 Problem Statement

Coal fines typically make up between 6 and 12 % of run-of-mine (ROM) material (Awan et al. 2022). With increased mechanization used in mines, many fines are formed which are discarded in stockpiles (Stonestreet & Franzidis, 1988; Botha et al., 2021). These fines pose health and environmental hazards as they cause land and water pollution. Acid mine drainage occurs during storage where sulphur-bearing minerals react with water and oxygen and seep into the ground polluting nearby underground water sources thereby becoming detrimental to the flora and fauna (Anawar 2015). An alternative way to utilise these coal fines is through GO production. GO and similar materials are being researched and applied across multiple fields, such as energy storage and production, novel composites, to healthcare and electronics. One of the major interests being that it can be a good alternative to Graphene in some applications.

Graphene has garnered significant interest owing to its unique structure and exceptional physico-mechanical properties (Moosa et al. 2021). Despite its advantages, graphene synthesis remains complex, and achieving uniform, large-scale deposition continues to pose challenges. In this context, GO emerges as a viable substitute, offering a more cost-effective and scalable production route. The strong hydrophilic characteristics of GO which makes is dispersible in aqueous solutions is attributed to inclusion of oxygenated functional groups like hydroxyl (-OH) and carboxyl (-COOH) (Razaq et al. 2022). This property also enables

GO to be modified, functionalized, dispersed in other solvents, deposited, and easily transported in contrast to pristine graphene (Sun 2019).

One such application of GO is in water treatment, particularly the removal of synthetic dyes in the growing industrial wastewater discharges. Dyes are persistent organic pollutants that are resistant to biodegradation and can pose significant environmental and health risks, including toxicity, carcinogenicity, and disruption of aquatic ecosystems. Conventional treatment methods are often ineffective or costly, making the development of efficient, affordable adsorbents crucial.

In this study, GO synthesized from coal fines is investigated for its potential to remove dye contaminants from wastewater. This aligns with global efforts to address water scarcity and pollution, challenges exacerbated by population growth, urbanization, and industrialization.

1.3 Aim and Objectives of the Study

The aim of the study was to synthesize graphene oxide from coal fines, for the development of a GO-based membrane, and evaluate its performance for the removal of organic dyes from contaminated water.

The objectives of this work were to:

1. Characterize the coal fines and evaluate their suitability for GO synthesis for membrane production and use for dye removal from water.
2. Characterize the structural and morphological properties of the synthesized graphite.
3. Compare the synthesized graphite to commercial graphite and verify its suitability for GO production.
4. Characterize the physicochemical properties of GO that were made through various Hummers' methods, through Scanning Electron Microscopy (SEM), Fourier Transform Infrared Spectroscopy (FTIR) and Raman Spectroscopy.

5. Evaluate the performance and efficiency of the nanofiltration membrane that was produced from graphene oxide (GO) fines for the removal of organic dyes from contaminated water.

1.4 Research Questions

The research questions addressed in this project were as follows:

1. What are the physical and chemical characteristics of the coal fines sample used for this experiment?
2. What will be the structural properties of synthesized graphite?
3. How will the synthesized graphite compare with commercial graphite already in the market?
4. Which Hummer's method produces graphene oxide of a higher degree in terms of oxygen content?
5. Can the synthesized graphene oxide membrane be effective when used to filtrate methylene blue organic dye?

1.5 Research Hypothesis

The thesis is hypothesised that the sample used in this study will have low moisture content, ash content, and volatile matter, as it was from the bituminous coal seam. Bituminous coal generally has lower moisture content, ash content and volatile matter as it is more mature than lignite and sub-bituminous coal. This is because it has undergone longer geological processes resulting in high carbon content and reduced impurities (Arnold 2023; Jovanovski, Boev & Makreski 2023). After graphitization, the expected product should be able to compare with graphite in the market as it will be synthesized under high temperatures, with a catalyst meeting the requirements for successful synthesis. The GO synthesized using an

optimized Hummers method is expected to contain abundant oxygenated functional groups, enhancing its hydrophilicity and dispersion in water. Consequently, the resulting GO-based membrane is anticipated to demonstrate effective removal of organic dyes from aqueous solutions, better than graphene membranes because of the existing oxygenated functional groups.

1.6 Significance of the Project

The success of GO production of a good quality of economic value would positively impact the coal industry as the coal fines in the stockpile would be utilised to promote good health to the communities around collieries. This is per Sustainable Development Goal 3 (SDG 3), which emphasizes promoting good health and overall well-being. The proposed method would be environmentally friendly and would help with wastewater treatment and purification. This is following Sustainable Development Goal 6 (SDG 6) concerning clean water and adequate sanitation. Industrialization and job creation can contribute significantly to achieving Sustainable Development Goal 8 (SDG 8), which promotes decent work and sustained economic growth. Owing to the heterogeneity of coal, this study is necessary as the quality of the synthesized GO is dependent on the carbon source used. The study also seeks to valorise coal fines from Morupule Colliery to produce both graphite and graphene oxide. Therefore, it seeks to find if the local coal fines would give GO of a good quality which can then be explored for industrial application including in wastewater treatment.

1.7 Thesis Structure

This work is divided into five distinct chapters.

Chapter 1

An introduction to the project, including its background, identifying the research problem, and presenting the primary objective, namely, the production of GO for application in water

treatment, is provided. Additionally, it highlights the study's significance to industry, particularly through the potential utilization of coal stockpiles and contributions to addressing water treatment challenges. This, in turn, aims to mitigate water scarcity issues both in sub-Saharan Africa and globally.

Chapter 2

It entails the literature review that reports on related works elsewhere on coal graphitization as well as production of GO using graphite through the Hummers' method. It helps identify the knowledge gap and hence stem more on the need and significance of the study.

Chapter 3

This chapter goes on to explain the methodology that was employed to carry out this study. Firstly, coal fines were used to synthesize graphite using metal-assisted microwave method followed by production of GO via Hummers method. The produced GO was employed for the production of membranes which were tested in water treatment. It was given in detail to enhance reliability, accuracy and replicability of the results obtained.

Chapter 4

This chapter presents the analysis of the data collected, examining it in the context of existing literature from related studies.

Chapter 5

It summarizes the key findings, outlines the conclusions derived from the research, and provides recommendations along with suggestions for future work aimed at enhancing and optimizing the results.

2 Chapter 2: LITERATURE REVIEW

This chapter gives a summary of the reviewed and analyzed literature concentrating on key points vital to assist in planning the experiment and finding the gaps in the study. The schematic in ***Error! Reference source not found.*** summarizes the significant areas of focus enroute to the production of GO from coal fines.

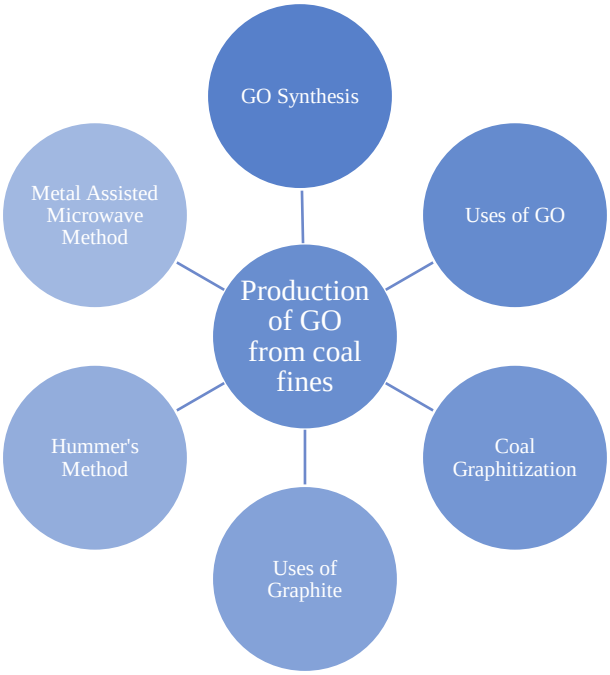

Figure 2.1: Literature review mind map.

2.1 Coal Fines

Coal utilization has been associated with climate change, air pollution, and human respiratory complications when combusted as a fossil fuel (Perera 2017). These findings have put pressure on the industry to finding alternative ways of utilizing coal. Coal is a carbon material with a very complex molecular structure as over a hundred levels of molecular structures have been presented (Hirsch & Backes 2010). It remains the most affordable and plentiful natural carbon source among conventional fossil fuels (Jovanovski et al. 2023). Coal fines are particles that feature in a size range of 1 µm to 1000 µm (Borowski & Hycnar 2013). These are mostly found in coal seams and dislodge during processing. With increased mechanization in

the field of mineral processing, fines generation increases tremendously with production (Stonestreet & Franzidis 1988). Geological factors also play a major role, especially given the coal deposits' physical characteristics, structure as well as their strength. Coal is a very heterogeneous material in both its physical and chemical structure (Orem & Finkelman 2013). It contains a variety of impurities, inorganic materials as well as organic materials comprising both non-volatile and volatile components which are introduced during its formation (Yadav & Lochab 2019).

Over the years, various studies have explored the utilization of coal fines such as, coal pyrolysis and briquetting (Massaro, Son & Groven 2014; Medupe et al. 2019; Lv et al. 2020) Increasing attention is now being directed toward converting coal-derived materials into high-value carbon-based products, including graphite, graphene, GO, and carbon nanotubes (Marcano et al. 2018). Given coal's status as the most abundant natural carbon source globally, it presents a viable raw material for production of Crystalline Graphite, a precursor for GO production and other significant applications (Tang et al. 2021).

2.2 Natural and Synthetic Graphite

Graphite is a polymorphic material that shows rhombohedral and hexagonal structure. Its crystal structure is made up of layers parallel to each other composed of condensed planar C_6 rings, as illustrated in ***Error! Reference source not found.***. Within each layer, atoms of carbon are bonded at angles of 120° to other three neighbouring carbon atoms bonded by weak van der Waals forces, forming a hexagonal arrangement. These interactions are responsible for the graphite's anisotropic behaviour (Jara et al. 2019).

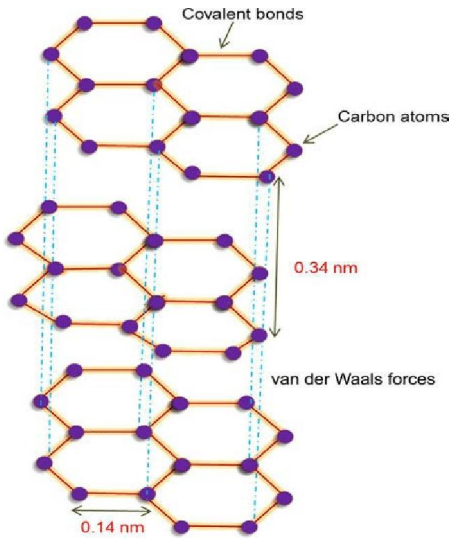

Figure 2.2: Graphite structure (Khan, Kausar & Ullah 2016)

Natural graphite is obtained through mining and subsequent processing, while synthetic graphite can be produced from a variety of carbon-rich sources. However, natural graphite is available only in limited quantities, and its extraction raises significant environmental concerns (Qiu et al. 2017). Synthetic graphite is derived through high-temperature treatment of materials like mesocarbon microbeads, petroleum coke, sponge coke, pitch, residual unburned carbon from fly ash, and anthracite coal (Ning et al. 2019). Typically, it undergoes heat treatment within the range of 2500°C–3000°C to yield highly structured or oriented graphite. Presently, various grades of petroleum coke are primarily utilized as filler material in production of synthetic graphite (Deng et al. 2022). Nevertheless, leveraging abundant coal fines presents a sustainable advantage in synthetic graphite production. Given the pollution concerns associated with natural graphite processing, transitioning coal into graphite stands as a promising alternative (Kim et al. 2016).

Natural graphite finds application in several industries, serving roles such as a lubricant, component in high-temperature gaskets, material for dense sealing layers, agent for suppressing metal fires, and as a thermal insulating medium for molten metals, conductivity

additives for electromagnetic reflectors, enhancing mechanical performance (Totton, Misquitta & Kraft 2011; Jara et al. 2019). From industrial applications like electrode manufacturing in aluminium and steel sectors to advanced technologies like fuel cells and lithium-ion batteries, synthetic graphite plays a vital role across various fields (Shi et al. 2021b). Its global utilization is on the rise, with exploration into applications traditionally reliant on natural graphite.

2.2.1 Coal Graphitization

Coal graphitization is a process of converting coal to graphite. Graphite derived from coal be produced using various high temperature treatment methods, resulting in a range of microstructures such as honeycomb, monocrystalline, polycrystalline, spherical, and rod-like (Islam et al. 2021). The production of graphite from organic materials includes two stages being carbonization and graphitization. Carbonization, which occurs from ambient temperature up to approximately 1000 °C is characterised by componential change where hetero-atomic impurities like hydrogen, sulphur, and nitrogen are removed leading to the formation of aromatic carbons skeletons theoretically (Li et al., 2021,Zhang et al., 2023). At temperatures between 1000-2000 °C (secondary carbonisation and pre-graphitization), heteroatomic content (S) are eliminated further. In graphitization (>2000 °C) growth of crystalline size and ordering in orientation occurs and graphite-like structures are formed as illustrated in ***Error! Reference source not found.***. It is important to highlight that in this process four forms of carbon nanostructures can be formed being, amorphous, polygonal concentric, graphite-like and pyrolytic graphitic nanostructures with varying degrees of crystallinity and order (Zhang et al. 2023).

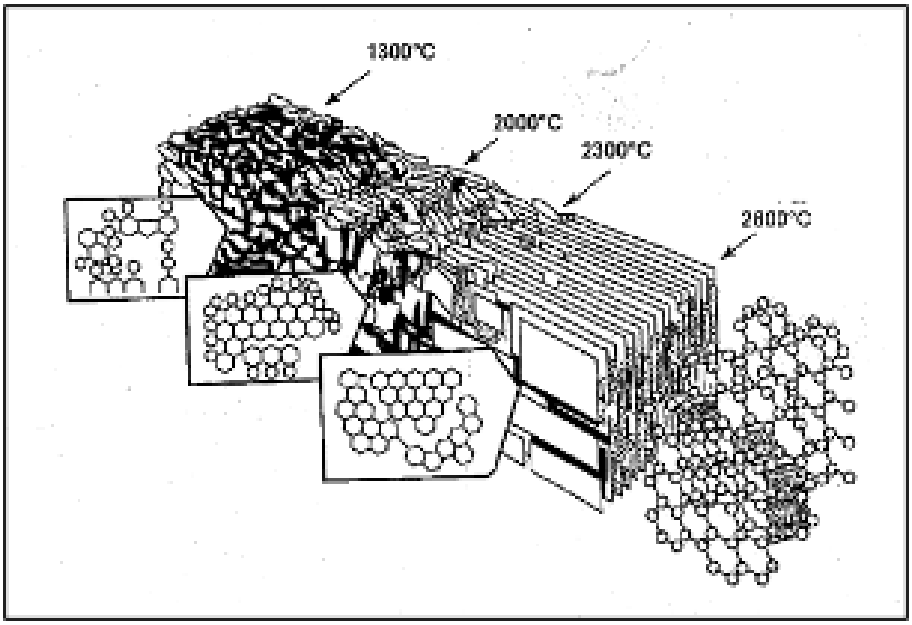

Figure 2.3: Structural changes of coal to graphite with temperature increase (Agarwal 2017).

Many ways have been used for graphitization, most employ the use of High Temperature Treatment (HTT) in a graphitic furnace (Islam et al. 2021; Khoshk Rish et al. 2021). In this method, a carbon rich substance (e.g coal) is fed into the graphite furnace which has a continuous flow of Argon (99.99 %) at temperatures above 2700 °C. One study applying this method involved the use of high-rank bituminous coal sourced a province in China called Shanxi to synthesize graphite. In this experimental procedure, the coal sample was first pulverised and then sieved to obtain particles smaller than 75 μm (Xing et al. 2018). This sample was carbonized in a tube furnace by heating it at 1000°C which had a continuous supply of Nitrogen for 4 hours. The obtained carbonized coal sample was then employed to examine how temperature affects the graphitization process. The temperature was varied at increments of +200 ºC from 2000 ºC to 2800 ºC, being the critical input variable (Xing et al. 2018). Shown in ***Error! Reference source not found.*** is a summary of studies done using HTT for graphitization, key findings and results obtained are highlighted.

Table 2.1: Methodology Table for Graphitization

Study	Purpose of Study	Methodology	Results
Viability of High-Temperature Graphitization for Deformed Low-Grade Coal. (Guo, Huan & Chen 2023)	Utilization of deformed coal as a feedstock for graphite synthesis instead of anthracite.	Graphitization using medium frequency induction graphitization furnace varying temperatures 2200°C and 2600°C under vacuum for meager coal and anthracite.	At 2200°C and 2600°C, a mylonitized meager coal, demonstrates superior graphitization capability. At 2200ºC (d002 = 0.3371 nm; G = 80.23%) reaches the semigraphite stage, whereas 2600ºC (d002 = 0.3364 nm; G = 88.37%) transforms into graphite.
Synthesis of Graphite from Bituminous Coal for High-Performance Lithium-Ion Battery Anode Materials (Xing et al. 2018).	Investigating the Impact of Temperature on the Graphitization Process.	A readily available and cost-effective bituminous coal was utilized as a precursor for the preparation of synthetic graphite materials via initial carbonization.	The results indicate that the microstructure of synthetic graphite materials is highly influenced by the graphitization temperature.
Structural Characterization of Graphite Materials Synthesized from Anthracite (González, Montes-Morán & Garcia 2003)	To investigate the impact of temperature, treatment duration, and initial coal particle size on the structural evolution of graphite materials prepared from anthracite at temperatures exceeding	Anthracite was first carbonized at 1273 K in a tube furnace, then graphitized at 2237 K in a separate furnace	At 1273 K, only minor structural changes were observed in the graphite materials produced. The initial size of the anthracite particles influenced the graphitization process

	2273 K.		with temperature, as it affected the ratio of organic to mineral content. Overall, the graphitization degree of this coal matched that of other natural and synthetic graphite.

The studies outlined in ***Error! Reference source not found.*** also shows that minerals and general feedstock in coal graphitization has influence in the final product. The studies exploring how presence of mineral matter in coal can impact graphitization shows that iron is most impactful. Iron has a positive effect, likely enhancing the formation of graphite structures within the coal matrix. In terms of influence of temperature, it has been notable that higher temperatures lead to increased graphitization (Xing et al. 2018). This observation aligns with thermodynamic principles as elevated temperatures provide the necessary energy for carbon atom rearrangement, fostering the development of graphitic structures in the coal matrix.

High-temperature treatment (HTT) presents a disadvantage due to high energy demand, and this has driven most research to finding alternative methods for coal graphitization without reliance on furnaces (Tang et al. 2022). This garnered explorative research in microwave technology. Recent investigations by Masi et al. demonstrated effectiveness by employing a one-step catalytic microwave treatment using copper foil which successfully converted coal powder into nano-graphite (Masi et al. 2021). Microwave treatments are favoured for their cost-effectiveness and efficiency.

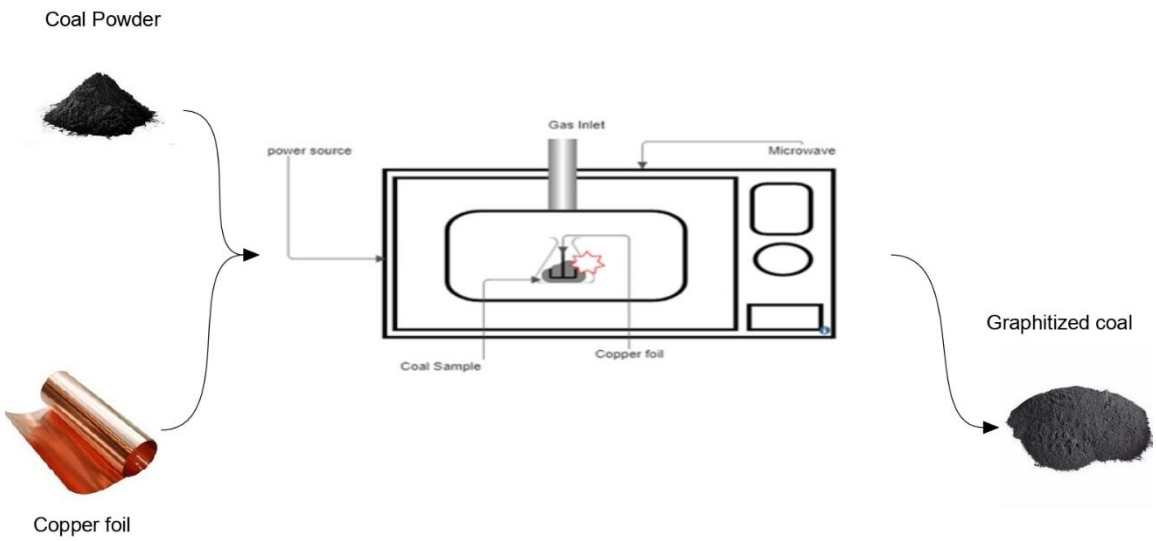

Figure 2.4 Schematic diagram of metal-assisted microwave graphitization.

Key factors in successful microwave-assisted treatments include high temperature, a reducing environment, a catalyst, and microwave radiation. Metal-assisted microwave treatment harnesses sparking of the copper foil that was fork shaped due to microwave radiation swiftly generating temperatures exceeding 1000 °C. To elevate temperatures further, metals with high melting points like tungsten, molybdenum, osmium, and rhenium can be utilized for spark induction (Masi et al., 2021). Achieving a reducing environment typically involves using 95 % Ar and 5 % H_2 gas. Microwave setups can employ a tube traversing the microwave region or a glass tube filled with Ar/H_2 gas (Islam et al. 2021).

2.2.2 Parameters in Coal Graphitization process

2.2.2.1 Temperature Influence

Graphitization demands high temperatures to overcome the substantial enthalpy associated with the transformation to graphite. This significant energy barrier remains one of the primary challenges impeding efficient graphitization (Hunter, Ramírez-Rico & Schnepp 2022). In a study by Wang et al, synthetic graphite with higher specific capacity and superior cyclic lifespan was prepared by graphitization of anthracite. Through thermal activation at

temperatures above 2800 °C, unstable carbon atoms were systematically transformed from a disordered state into an ordered graphite crystalline structure (Wang et al. 2020). The slow reaction speed and low temperatures leads to poor graphitic structure development, consistent with the findings of (González et al. 2003). In the work carried by Gonzalez et al, temperature was put to test to investigate the crystallinity of graphite produced after graphitization of anthracite in a graphitization furnace. The results obtained from the XRD indicated that highly crystalline material was obtained at 2673K compared to the material obtained at temperatures of 2473 K and 2573 K (González et al., 2003).

The use of catalytic agents can allow for graphitization at lowered temperatures and hence overcome high energy consumption. Acheson introduced the term catalytic graphitization and to date, catalysts have been used to aid graphitization (Wang et al., 2020). Catalysts used in the graphitization process are generally classified into three categories: elemental metals (such as Fe, Ni, Ti and V); metal compounds (Fe_2O_3, FeO, Fe_3O_4, Cr_2O_3, MnO_2) and alloys (Fe-Si and P-Ni) (Yang et al. 2022). The catalytic effect of alloys has been found to have better effect relatively due to their low melting point. This results in a low temperature for catalytic graphitization, with the process beginning as low as 400 °C (Krishnan et al. 2014).

B_2O_3 and Fe_2O_3 are one of the most used catalysts (Hunter et al. 2022). Boron atom is an electron-defiant atom which has the strong tendency to attract electrons, facilitating the absorption of cationic species. This interaction can break covalent bonds, leading to the formation of boron carbide. Boron carbide decomposes in high temperature treatment into boron and graphitized carbon (Khoshk et al., 2021). This mechanism also applies when working with Fe_2O_3 as a catalyst. The two main mechanisms followed by catalytic graphitization are dissolution precipitation and carbide formation decomposition (Islam et al. 2021). Khoshk et al used B_2O_3 as a catalyst and observed that coal with the catalyst had graphitization of 83.7 % compared to 55.8 % of no catalyst whist working at the same

temperature of 1800 °C. Tang et al used reduced iron particles in form of Fe_2O_3 as a catalyst to graphitize anthracite working at 2400 °C and Fe_2O_3 content of 20 % and the resulting graphite achieved a graphitization degree of 96.51 %. In Fe-assisted graphitization, the continuous interaction between iron and carbon through the creation and breaking of C-C and Fe-C bonds promotes the rearrangement of carbon atoms. This process transforms non-hexagonal rings into regular six-membered aromatic rings, with iron acting as a structural mediator to enhance graphitic ordering over time. (Tang et al. 2022).

Additional research has shown that carbon materials can also act as catalysts for graphitization at low temperatures. (Barnakov et al. 2015) studied iron salt and needle coke and as catalyst for graphitization of coal tar pitch at low temperatures. In the carbonization of coal tar pitch with the addition of selected catalysts, the resulting material exhibited a greater graphitization degree and larger crystallite sizes compared to those produced from the carbonization of pure pitch alone. Among the catalysts investigated, foamed graphite demonstrated the greatest catalytic activity. Notably, when foamed graphite was used at temperatures between 800 - 900 °C, the resulting carbon material displayed a crystalline structure comparable to that of native graphite. In contrast, the carbon material derived from coal tar pitch without any catalyst remained largely amorphous (Barnakov et al. 2015).

2.2.2.2 Mineral matter influence

Coal mineral matter has also shown to have influence in the graphitization process by acting as a catalyst. In a study by Shi et al, more-ordered materials were prepared from anthracites with a higher H/C atomic ratio when using B_2O_3 was used as a catalyst (Shi et al. 2021a). This was beneficial for the growth of the aromatic layer in graphite structure, reduced cross-linking, enhanced coplanarity, and lowered the energy barrier for graphitization, speeding up graphite formation (Shi et al. 2021c). When comparing the chemical structure of anthracite and bituminous coal, bituminous coal contains a relative high amount of volatile matter (Ning

et al. 2019). This can serve as a big advantage during production to make the carbon matrix porous during high-temperature treatment. Most mineral components begin to decompose around 1500 °C and escape as gases or liquids and as the temperature rises to 2200 the mullite undergoes decomposition. Upon reaching temperatures around 2700 °C, only trace amounts of silicon remain, acting as a residual catalyst within the high-temperature environment. (Wang et al. 2021).

Studies have shown that the particle size of the starting material, in this case coal, have an influence in the graphitization process due to variations in the distribution of organic and mineral matter (Gonazález et al. 2004; Qiu, Yang & Bai 2020; Chen et al. 2022). The level of graphitization achieved has been shown to be similar to that of natural and synthetic graphite. Crystallinity is typically evaluated through X-ray diffraction (XRD), using the interlayer spacing (d_{002}), crystallite height (Lc), and lateral size (La) (Qiu et al. 2019). Complementary characterization techniques, including Raman spectroscopy, SEM, TEM, and nitrogen adsorption–desorption analysis, to assess the structural and surface properties of the synthesized graphite materials (González et al., 2003).

2.3 Graphene Oxide Synthesis

GO has a hexagonal carbon structure similar to that of graphene, but also contains various oxygenated functional groups such as hydroxyl (-OH), alkoxy (C-O-C), carbonyl (C=O), carbox-ylic acid (–COOH) as shown ***Error! Reference source not found.***.

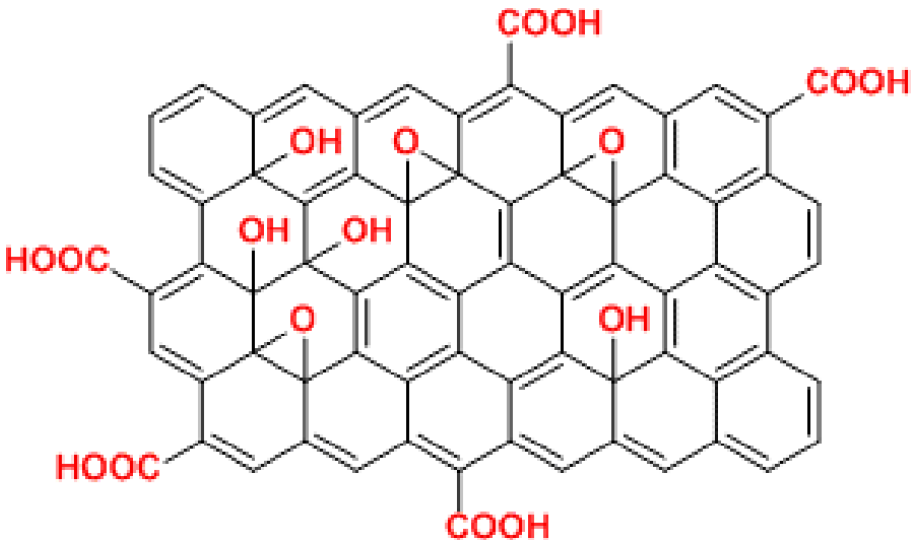

Figure 2.5: Showing the Graphene Oxide Structure (Lerf et al. 1998)

British chemist Sir Benjamin Collins Brodie discovered properties of GO through a theoretical analysis of the structure of graphite and its oxidised version (1859). Ludwig Staudenmaier later corroborated this postulation, and it has been popular among researchers since then (Zaaba et al. 2017). In 1898, Ludwig Staundenmaier enhanced Brodie's method by replacing 2/3 of fuming nitric acid, with sulfuric acid and by adding multiple aliquots of potassium chloride, during the reaction (Li et al. 2019). Subsequently, chemists Hummer and Hofmann introduced several safety improvements to the original methods, such as using potassium permanganate ($KMnO_4$) as an oxidizer instead of potassium chlorate ($KClO_3$), which releases toxic ClO_2 gas, and incorporating sodium nitrate ($NaNO_3$) (Smith et al. 2019b).

Currently, the Hummers method is preferred due to its safety and scalability. GO is synthesized using a carbon precursor which is dispersed in a strong acid as well as an oxidizing agent like potassium permanganate to kickstart the process of oxidation (Chen et al. 2013; Surekha et al. 2020). This process is usually stopped by addition of hydrogen peroxide H_2O_2 to the mixture (Chen et al. 2013; Alam, Sharma & Kumar 2017). The solid product is

then separated and purified using dilute hydrochloric acid to further remove remaining impurities (Chen et al. 2013). GO synthesis is essentially divided into 2 categories, bottom-up method (coal to GO) and top-down (coal to graphite, then GO synthesis). However, in this case, coal will be used as a precursor for the synthesis of graphite which will then be exfoliated for the production of GO, a top-down approach. Bottom-up synthesis methods, while precise, tend to be time-consuming and present notable challenges when scaled beyond laboratory settings (Chen et al. 2015).

The other popular modification of GO synthesis is improved Hummer's method. It eliminates the release of toxic gases, allows for better temperature control during the reaction, and produces GO with a higher oxygen content. Sodium nitride (Na_3N) is replaced with phosphoric acid and $KMnO_4$ is added (Chen et al. 2013). The average dimensions of synthesized GO sheets are greatly affected by the morphology of the precursor material (Chen et al. 2015; Lacina et al. 2018).

Summarised in ***Error! Reference source not found.****.2* is a comparative evaluation of different techniques entailed in the production of GO from various raw materials.

Table 2.2 Methodology Table for Graphene Oxide

Study	Purpose of Study	Methodology	Results
An improved Hummers method for eco-friendly synthesis of graphene oxide (Chen et al. 2013)	To compare GO produced with the convectional Hummers method and Improved Hummers method	An improved Hummers method without using $NaNO_3$ was used to produce graphene oxide	GO produced had the same chemical structure, dispersibility, thickness and lateral dimension, nonetheless, the improved method offered the advantage of no emission of NO_x gases.
Graphene oxide	Investigates the structure	Two types of GO	The shorter reaction time (20

synthesis using microwave-assisted vs. modified Hummer's methods: Efficient fillers for improved ionic conductivity and suppressed methanol permeability in alkaline methanol fuel cell electrolytes(Shi et al. 2021c)	and characteristics of microwave-assisted graphene oxide (denoted as MGO) nanofillers and their effect as membrane electrolyte assembly for the fuel cell.	nanosheets are fabricated: MGO and modified Hummer's method (denoted as NGO)	min) of the microwave method also generated larger GO sizes than the conventional method
Bioinspired graphene oxide nanofiltration membranes with ultrafast water transport and selectivity for water treatment (Yang et al. 2022)	Interlayer interactions and poor mechanical stability of graphene oxide (GO) membranes pose significant challenges in any practical application environment	The synthesized GO-chitosan (GO-CS) composites with covalent bonds by a one-step hydrothermal method, and prepared a series of composite membranes using vacuum filtration	The presence of covalent bonds between GO and CS resulted in significantly enhanced membrane stability
A critical review on graphene oxide nanostructured material: Properties, Synthesis,	Review paper examines the properties, preparation methods and characterization techniques for graphene oxide (GO) nanostructured materials.	Review of existing literature	The presence of graphene oxide nanostructured materials in composite material enhanced the overall performance in their respective applications

characterization and application in wastewater treatment (Ajala et al. 2022)			

Comparative studies on different GO synthesis methods continue to be undertaken, for instance, in a recent study done by researchers in China, two different samples of GO were synthesized using two techniques; being the improved as well as the modified hummers method (Sohail et al. 2017). It was noted that samples produced by both methods exhibited nearly identical physicochemical properties. Spectral analyses revealed an optical band gap of 3.1–3.9 eV, while thermal stability was observed up to 550 °C. XRD confirmed a semicrystalline structure with crystallite sizes between 27–28 nm. Dielectric studies revealed reduced activity at lower frequencies due to interfacial polarization, while higher-frequency activity was attributed to dipole relaxation. Based on these results, the synthesized GO was suggested for use in capacitors and composite materials that are thermally (Sohail et al. 2017). This indicates that different fabrication methods can precedes the intended application of the GO to be produced.

2.4 GO membranes for water treatment (dye removal)

The extensive application of organic dyes across industries like paper, paint, leather, and textiles result in the generation of large volumes of wastewater containing these dyes (Prakash 2022). Given that many of the used dyes are toxic, non-biodegradable, and some have been proven to be carcinogenic, it is crucial to remove them from water to mitigate the risks they pose to the health of humans and the environment (Yang et al. 2020). Different methods such as physical biosorption, chemical precipitation, and membrane filtration have

been devised for dye removal (Gadekar & Ahammed 2016; Gadekar & Ahammed 2019). The use of filtration membranes is particularly popular because of their high separation efficiency, environmentally friendly and compact design (Ma et al. 2020).

GO-based membranes have attracted attention in recent years for use in water treatment due to their excellent mechanical strength, lamellar structure and single- atom thickness (Mouhat, Coudert & Bocquet 2020; Yang et al. 2022; Sahoo et al. 2024) . The oxygen functional groups on their surface not only enhance water permeation but also improves the selective rejection of contaminants due to their negatively charged surface (Ma, Ping & Dong 2017). Membrane filtration has demonstrated to be a viable substitute to traditional methods like distillation, crystallization, and condensation (Chong et al. 2018). It is easy to operate, energy-efficient, and does not generate secondary pollution or require additional chemicals such as coagulants and flocculants, making it an ideal solution for water treatment. Different fabrication methods such as vacuum filtration, layer-by-layer (LBL) self-assembly, spin-coating, and dip-coating can be used for fabrication of GO membranes.

2.5 Research Gaps

Currently most of research is concentrated on synthesis of GO directly from coal or graphite and hence there is a notable gap in exploring the full process of converting coal to graphite before synthesis of GO. Graphite is also a highly versatile material that has broad applications such as in battery technology, lubrication and pencil production. Most studies have concentrated on utilizing graphite-derived GO to create membranes for applications such as dye removal, but few have investigated the potential of coal-derived GO for this application. My research seeks to address this gap by first converting coal into graphite and then synthesizing GO through the Hummers method. This novel approach may open the door

to usage of coal as a feedstock for both graphite and GO production, with potential advantages in material performance and scalability. Moreover, the feasibility of employing coal-based GO in membrane technologies for dye removal has been largely unexplored. By analyzing the properties and performance of coal-derived GO membranes, this research aims to advance the development of more affordable and sustainable solutions for wastewater treatment and environmental remediation, particularly in coal-rich regions like Botswana.

3 Chapter 3: METHODOLOGY

This chapter will give a brief overview of how the work in the thesis was conducted giving essential steps that were undertaken to complete the study. This chapter includes research materials, equipment, a procedural description of the experiments conducted, and characterisation undertaken from coal preparation, GO fabrication and tests in water treatment.

3.1 Materials

The sample used for this study was coal fines that were discarded and stockpiled in a colliery in Palapye, Botswana. The process of coal graphitization involved employing Fe_2O_3 as a catalyst, a Defy 30 L household microwave, and 30 µm copper foil. GO was synthesized from the prepared graphite using potassium permanganate ($KMnO_4$), concentrated sulfuric acid (H_2SO_4, 99 %), dilute hydrochloric acid (HCl, 10 %), and hydrogen peroxide (H_2O_2). All chemicals were procured from Sigma Aldrich (SA). For water treatment test methylene blue was used to test the efficiency of the GO membranes.

3.2 Methods

A sequential summarised representation of the research design from the collection and sampling of coal fines to wastewater treatment using GO is represented in ***Error! Reference source not found.****1*. The GO produced was intended for use in treating wastewater contaminated with organic dyes.

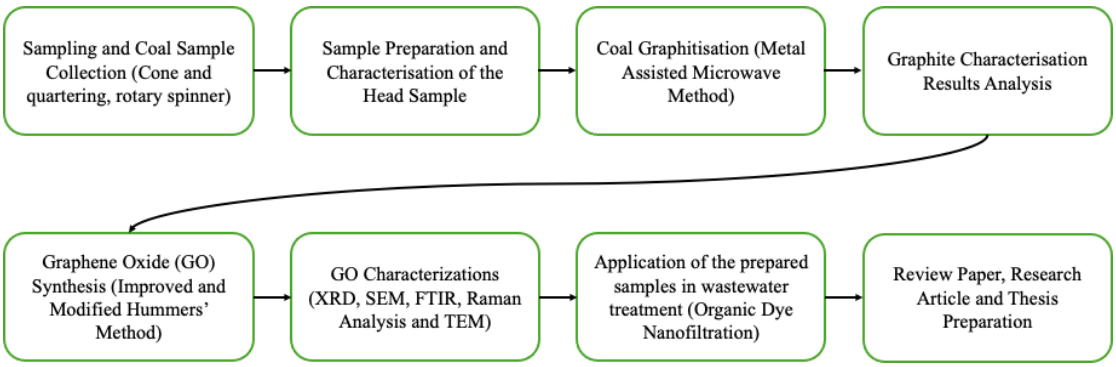

Figure 3.1: Shows the Research Design flowsheet.

3.2.1 Sample collection, preparation and characterization.

Coal fines sample of 2 kg was received and had a 70 % passing 4.5 mm. Representative samples were obtained from the head sample using sampling methods such as cone and quartering, splitting riffle and rotary splitter. A representative sample of 50 g was obtained and prepared for characterization by proximate analysis in accordance with the American Society for Testing and Materials D3176-15 (ASTM D3176-15. 2015) guidelines as well as Raman spectroscopy, FTIR, and SEM techniques (ASTM, 2015; Pavia et al., 2015;Goldstein et al., 2017) . These analysis aimed to analyse the quality of the obtained coal in terms of physicochemical characteristics. Illustrated in ***Error! Reference source not found.*** is the sequential depiction of the methodology that was employed in this project. It shows the initial step which involved taking a representative sample of the bulkhead sample for graphitization. Prior to graphitization, this coal sample was carbonized inside a nitrogen atmosphere at 1000 °C for a period of 2 hours. After carbonization the sample underwent graphitization using the metal-assisted microwave method. The product obtained after graphitization was used in the production of GO incorporating different modifications of Hummers' method.

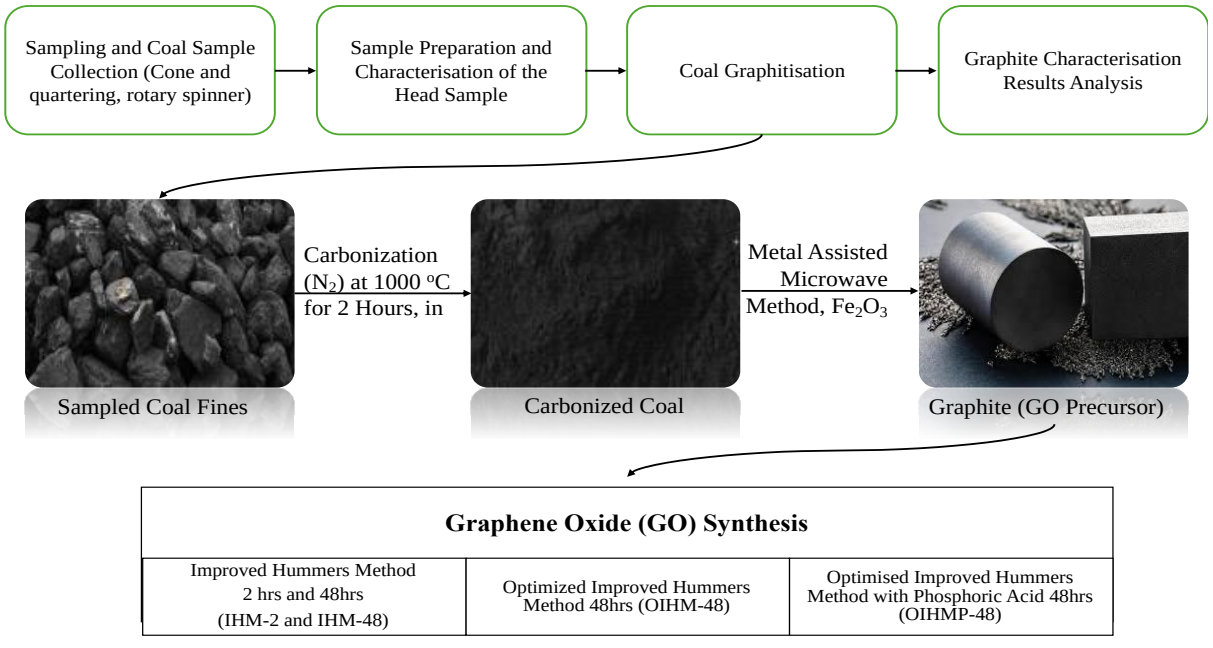

Figure 3.2: Sequential representation of the preparation of GO from coal fines.

3.2.2 Coal graphitization process

For coal graphitization, a sample of 500g was obtained from the head sample and pulverized and placed in graphite crucibles for carbonisation. This process was carried out inside a tube furnace at a heating rate 5 °C per minute to 1000 °C for two hours. This process was completed under an inert nitrogen atmosphere to remove volatile compounds (Zhuo, Xie & Shen 2021). Carbonisation is a vital pre-graphitisation step, as it eliminates volatile matter that could introduce defects during graphitisation and forms a porous carbon matrix, which facilitates carbon atom diffusion in subsequent catalytic graphitisation (Kumari 2020).

Following carbonisation, a mixture of 9.5 g carbonised coal and 0.5 g Fe_2O_3 catalyst was exposed to microwave radiation using a household microwave. Fork-shaped copper foil acted as a sparking agent, and the radiation lasted 15 minutes. At temperatures exceeding iron's melting point (1538 °C), microwave-induced sparking in copper foil leads to the volatilisation of elemental iron from $Fe_2\ O_3$ (Hunter et al. 2022). Iron readily reacts with carbon to form intermediate iron carbide compounds (FexCy), which decompose into graphitizable carbon (Qiu et al. 2019; Shi et al. 2021c). This carbon subsequently transforms into crystalline graphite under the high temperatures generated by sparking (Masi et al. 2021). After cooling the sample in a desiccator, metallic iron was separated magnetically, while residual trace elements were leached using hydrochloric acid with assay of 37 % at room temperature for three hours at 200 rpm. This leaching step removes iron residues and prevents oxidation (Islam et al. 2021). The sample was then washed with deionised water to obtain a neutral pH and oven-dried at 50 °C overnight in preparation for analysis. For comparison, raw coal and pure graphite were also analysed to confirm successful graphitisation.

3.2.3 Graphene Oxide synthesis using Hummers Method

Graphene oxide was synthesised using 5% Fe_2O_3 graphite of different versions of the Hummers methods elaborated as follows. The synthesized graphite material underwent GO production through various Hummer's methods. The used methods were the Improved Hummers' method where there were oxidation times of 2 and 48 hours (IHM-2 & IHM-48). The remaining two methods employed were variations of the Optimized Improved Hummers method, both involving a 48-hour oxidation period, one incorporating $NaNO_3$ (referred to as OIHMNa) and the other excluding it (OIHM48). For IHM-2, 10 grams of graphite were mixed with 250 mL of H_2SO_4 in a beaker and heated to 50 °C. $KMnO_4$ was slowly introduced into the mixture, which was then stirred at 200 rpm for a duration of 2 hours. Potassium Permanganate and sulphuric acid are oxidising agents that would introduce the oxygenated functional groups in graphite forming graphite oxide and for exfoliation which widens the d-spacing in graphite (Chen et al. 2013; Chen et al. 2022). The reaction was completed by adding H_2O_2 and HCl, followed by filtration and rinsing with deionized water. Hydrochloric acid was added in order to stop any MnO_2 oxidation.

The final mixture was sonicated for 30 minutes to enhance the uniqueness of the GO nanosheets using Fisherbrand FB1505, Elmasonic S30 H. The similar procedure was carried out for the IHM48 sample, where the sample was treated with H_2SO_4 and $KMnO_4$ for 48 hours instead of 2 hours. The resulting sample was then dried and analyzed. For OIHM-48 experiments, a 500 mL beaker containing 100 mL of H_2SO_4 and 10g of graphite was used. The solution was kept in an ice bath for 2 hours to ensure the temperature remained below 15 °C and then raised to 35°C. $KMnO_4$ was gradually added and stirred for 48 hours at 300 RPM. The heat was increased to have the temperature at 98°C and maintained for 30 minutes, followed by the addition of deionized water until effervescence ceased. Oxidation was stopped using 10 mL H_2O_2 and 50 mL 10% HCl. After cooling, the mixture was rinsed with

deionized water, and the final solution was sonicated for 30 minutes followed by drying and analysis. For OIHMNa-48, the previous steps were followed for OIHM-48 however, 12 grams of $NaNO_3$ was dissolved in H_2SO_4 before adding the 10 grams of graphite powder to act as a catalyst during oxidation.

3.2.4 GO Membrane Fabrication

Graphene Oxide (OIHM48-GO) membranes were prepared through the vacuum filtration technique on Polyacrylonitrile (PAN) and Polycarbonate (PC) substrates. The size of the pores on both substrates was 0.45 µm. The membranes were prepared by making a solution of GO powder with distilled water at concentrations' of 0.05, 0.1, 0.3, 0.5, 0.7, and 1.0 mg/mL. To guarantee the consistency and delamination of GO sheets, the solution was first sonicated for 30 minutes before vacuum filtration (Xia et al. 2013).

The substrates used were rinsed with distilled water before being placed in the filtration unit. The GO solutions were dispensed onto the membrane filter and the vacuum pump was activated to filter the GO solution through the membrane. This process created a thin GO film on the substrate and was repeated for each concentration on a new substrate and the GO coated membranes were dried overnight in an oven at 25°C.

3.2.5 GO Membrane performance tests

To study how different concentrations of GO have an impact in water treatment, the membrane's ability to filter methylene blue (MB) solutions were used. The procedure involved using a dead-ended filtration cell as shown in **Error! Reference source not found.** to filter a 10ppm methylene blue solution.

3.2.5.1 Nanofiltration Setup:

To test the validity of the made-up membranes, they were mounted on a polyethylene disc providing with a filtration area of 13.20 cm^2. Neoprene gaskets sealed the filtration cell, which was pressurized with inert nitrogen gas. The procedure was carried out using minimum pressure of 1 bar. The performance of the membranes was evaluated with increasing GO concentration by filtering 100 mL of aqueous methylene blue solution with a concentration of 10 mg/L through each of the vacuum filtration fabricated membrane. The solution was introduced through a feed inlet and pressurized air assisted filtration through various GO membranes as shown in **Error! Reference source not found.**. During post-filtration, the permeate was analysed to compare the concentration of methylene blue before and after filtration.

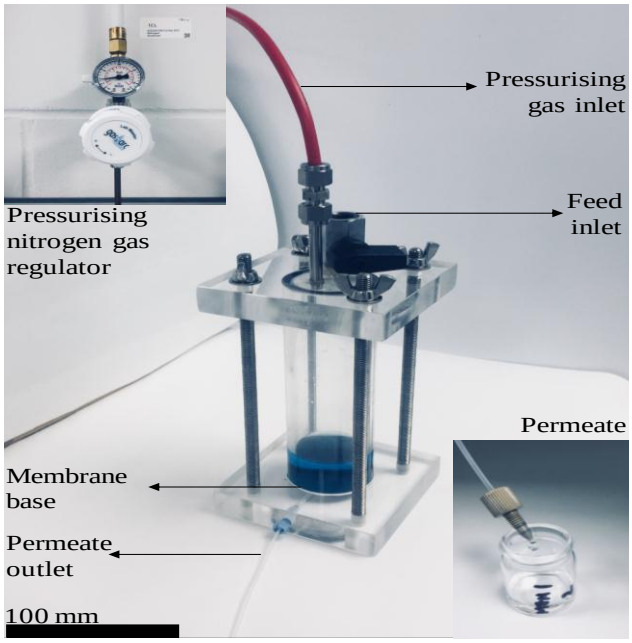

Figure 3.3: The operational setup of the custom-built nanofiltration cell unit.

3.3 Methods of analysis (Physicochemical Characterisations)

3.3.1 FTIR Spectroscopy Molecular Characterization

FT-IR Spectroscopy a non-destructive technique that analyses functional groups by detecting molecular vibrations, offering comprehensive information on the chemical structure of graphite and GO obtained (Zhang et al. 2023). The model used was DW-FTIR-530A. Approximately 2 mg of finely ground sample was mixed with potassium bromide (KBr) and pressed into a pellet using a hydraulic press. The spectra were recorded in the range of 4000-400 cm^{-1} with a resolution 4 cm^{-1}, and 32 scans were averaged per sample. Baseline correction and normalization were applied before interpreting the spectra.

3.3.2 SEM – Morphological Analysis

SEM was utilized to establish the morphological structure using SEM "SIGMA". The samples were mounted onto a conductive adhesive layer, placed in the sample holder, and subjected to analysis The SEM analysis was conducted under high vacuum at an accelerating voltage of 5 - 20 kV, with images captured at varying magnifications to assess morphological changes.. This technique enabled observation of the structural transition from amorphous to more ordered or crystallized forms in irradiated samples, consistent with previous findings (Xia, Yang & Liang 2014).

3.3.3 Raman Spectroscopy – Structural Characterization

This was applied to ascertain transformation of the amorphous coal structure into a crystalline graphitic form (Schuepfer et al. 2020; Li et al. 2022). The structural disorder in the carbon material is evidenced by the presence of the D band (1350 cm^{-1}) whilst the degree of graphitic order correlates to presence of the G band (1580 cm^{-1}). The intensity of these bands (I_D/I_G), denoted as *R*, is mostly used to assess the level of disorder in the structure, with low values indicating a more ordered structure and high values indicating a less ordered

carbon structure (Khoshk Rish et al. 2021). The equation used is as shown below, $R = \frac{ID}{IG}$ *Equation 3.1*.

$$R = \frac{ID}{IG} \qquad \textit{Equation 3.1}$$

The inVia-Reflex micro confocal laser Raman spectrometer with laser output power of 20 mW and excitation wavelength of 532 *n*m was used in this study to determine the degree of graphitization.

3.3.4 Characterization of fabricated membranes

3.3.4.1 Equilibrium Water Content (EWC) and Membrane porosity

These are critical parameter in sectors of drug delivery systems, tissue engineering and water filtration (Wei, Peng & Xu 2014). It refers to the maximum amount of water that a hydrophilic membrane can absorb and retain when it reaches a stable state under specific conditions (Lyu et al. 2018). EWC was determined by evaluating the water uptake of the membrane using the soaking technique. Dried membranes were weighed and subsequently placed in deionized water for 24 hours until saturation. After soaking the membranes were mopped carefully with tissue paper to remove excess water in the surface and it was weighed. These were used to calculate the EWC using Equation 3.2 expressed in percentage.

$$EWC = \frac{Weight\ of\ wet\ membrane - weight\ of\ dry\ membrane}{weight\ of\ dry\ membrane} * 100 \qquad \textit{Equation 3. 2}$$

Porosity is related to Equilibrium water content and can be used to assess the membranes hydrophilic or hydrophobic properties (Rezaee et al. 2015). To determine the membrane porosity, it was measured using gravimetric method based on membrane mass loss after drying. These membranes left to dry in an oven set at 60 °C overnight. Afterwards the membranes were weighed, and the porosity was calculated from Equation 3.3.

$$E(\%)\frac{Wo-W1}{A*l*dw}*100$$ *Equation 3.3*

Here, W_0 and W_1 (g) correspond to the masses of the membrane in wet and dry conditions, respectively, d_w indicates the density of water (g/cm^3), A refers to the effective surface area of the membrane (cm^2), and l represents the thickness of membranes at wet state (cm).

3.3.4.2 Permeate Flux and Rejection rate

Key performance metrics, including permeation flux (F) and dye rejection rates, were determined for each membrane to assess their efficacy. The permeate flux was determined for all the membranes at 1 bar and the pure water flux was recorded. Crossflow filtration unit was employed by filtrating distilled water through a membrane of active area 13.20 cm^2 at a set pressure of 1bars, 23 ± 1 °C and 0.22 m/s crossflow velocity. The experiments were conducted with compressed nitrogen gas. The permeate flux was subsequently computed at different transmembrane pressures using the Equation 3.4 where F = permeate flux (expressed in L/m^{2}h-1), Vp = volume of permeate (L), A = area of the membrane (m^2) and Δt = time (h).

$$F = \frac{Vp}{A*\Delta t}$$ Equation 3.4

The membranes' rejection rate was evaluated by filtering dye solutions with varying molecular weights under a pressure of 1 bar. Membrane percentage rejection [R] was calculated using Equation 3.4 where C_p and C_f are the concentrations of permeate and feed. These concentrations were determined using UV-Vis characterizations (Hitachi U-3900 UV-Vis) by comparing the absorbance of the permeate solutions to that of the feed. A calibration curve was constructed to enable concentration-based calculations of methylene blue (MB) rejection. As shown in **Error! Reference source not found.**, this curve was derived from

three sets of absorbance concentration data and averaged to produce a calibration line that falls within the linear range of the Lambert-Beer law.

$y = 0.1987x$ Equation 3.5

$R\text{^}2 = 0.1981$

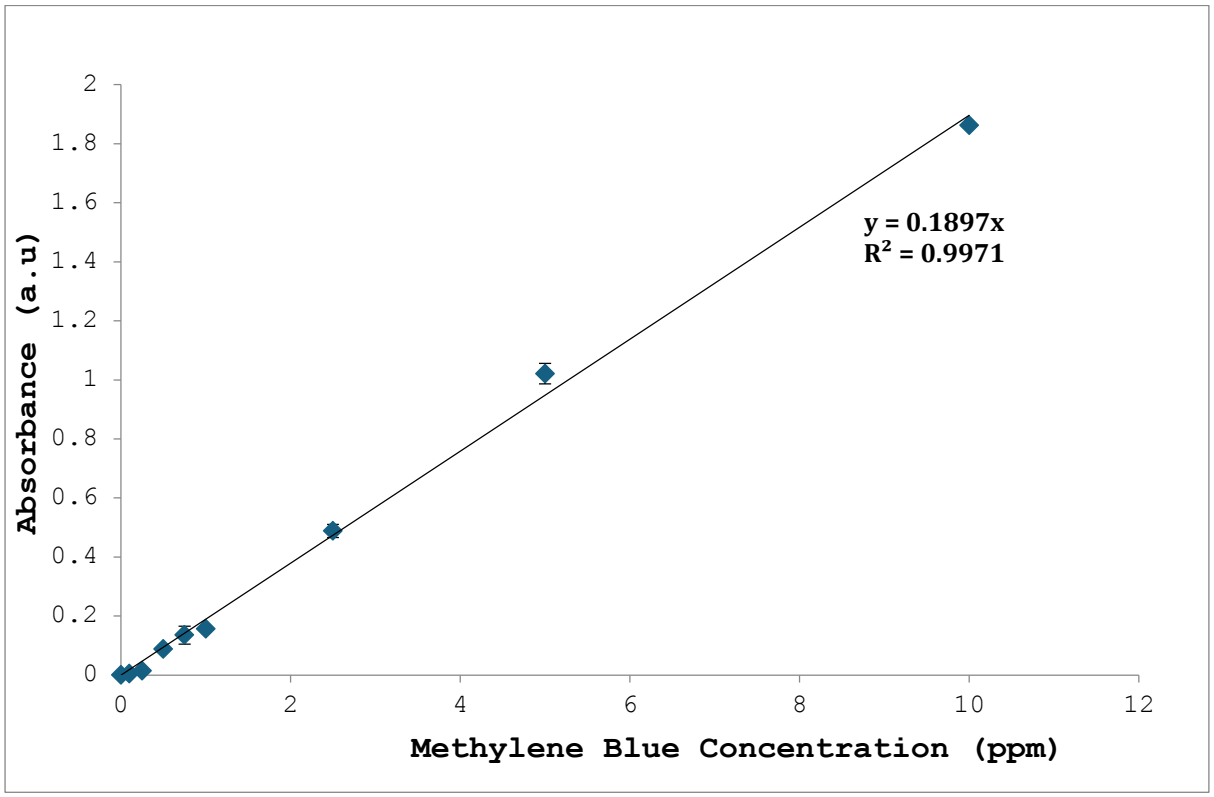

Figure 3.4: Overall calibration line.

To ensure that the obtained results are accurate, this test was done three times on three membranes using the same conditions and the concentration based MB rejection was calculated. The standard deviation of the nanofiltration data was recorded for both the average flux and rejection percentages.

$$R\ (\%) = \left(1 - \frac{Cp}{Cf}\right).100$$ *Equation 3.6*

3.3.4.3 Membrane hydraulic resistance & fouling resistance

The ease at how water flows through the membrane is quantified as hydraulic resistance (Xu et al. 2014) . It can be measured using the pressure drop across membranes while filtering at a constant flow rate when using dead-end filtration. It will then be calculated using equation 3.7, where ΔP represents the pressure drop and Q represents the volumetric flow rate;

$$R = \frac{\Delta P}{Q} \qquad \textit{Equation 3.7}$$

Fouling resistance (Rp) in the membranes arises from the plugging of pores and irreversible adsorption of foulants on the membranes surface. This property hence probes assesses the membranes ability to resist fouling over time (Sarihan & Eren 2017). It can be calculated and modeled using equation 3.8 where J_f is the final flux and J_i is the initial flux. This flux recovery ratio can be used to evaluate the antifouling properties of the membranes.

$$Rp = \frac{1}{Jf} - \frac{1}{Ji} \qquad \textit{Equation 3.8}$$

4 Chapter 4: RESULTS AND DISCUSSION

Entailed in this section is the raw and analysed results obtained, as well as discussion of these findings. It also gives correlation between hypothesis and findings in comparison to other related work.

4.1 Characterization of the coal sample

The results obtained from the proximate analysis of the coal samples are presented in Table 4.1 showing that the sample used for this study had high ash content of 17.73 %, which is significantly higher compared to the ash content of bituminous coal which usually ranges between 6-9 % (Li et al. 2016). Coal of such high ash content is indicative of lower coal quality, as ash does not contribute to the calorific value (CV) and can negatively affect combustion efficiency and increase waste disposal costs. Similar high-ash coal samples have been reported in studies from India and South Africa, where certain lignite and sub-bituminous coals were found to have ash contents in the range of 15-25 % due to mineral inclusions and geological conditions (Rath et al., 2014; Moolman et al., 2019).

The coal sample also has volatile matter (VM) content of 28% which falls within the expected range of low rank bituminous coal, and aligns closely with results of low rank bituminous coal from Shian China of range 23-29 % (Yi et al. 2017). A high VM suggests ease of ignition and potential suitability for thermal applications, though it may also imply lower thermal stability and more volatile emissions. The fixed carbon (FC) in this sample was calculated to be 50.75 %, which is lower than typical bituminous coals (which range from 60-80 %). This FC aligns well with sub-bituminous coals, which generally have fixed carbon in the range of 50-60 % (Speight, 2013). This further supports the classification of the sample as low-rank sub-bituminous. The moisture content of 3.52% is relatively low and favourable for combustion, as high moisture reduces heating value. Comparable moisture values have been

reported in thermally matured sub-bituminous coals used in power generation in parts of Eastern Europe and Indonesia (Kusrini et al., 2018).

From a practical standpoint, this type of coal may still be suitable for industrial boilers or thermal power plants. The high volatile matter supports its potential use in gasification or combustion applications, although the ash content could result in slagging and fouling issues during use, requiring careful process design or blending with higher quality coal.

Table 4.1: Proximate analysis results for raw coal sample.

Ash	Volatile Matter (VM)	Fixed Carbon (FC)	Moisture
17.73%	28%	50.75%	3.52%

4.2 Coal Graphitization

4.2.1 Raman Analysis

The Raman spectra of raw coal and graphitized coal sample after metal assisted microwave treatment are illustrated in Figure *4.1*. In Raman spectra at 1350 cm^{-1} is the D peak, observed in the first order region and signifies the presence of amorphous aromatic structures or vacancy defects (Zhang et al. 2019). This peak is typically inactive in highly crystalline graphite but becomes noticeable in coal and polycrystalline graphite due to structural disorder and edge effects (Omoriyekomwan et al. 2019). Graphite exhibited characteristic peaks, being the G peak at 1580 cm^{-1} which reflect the graphite's structural order (Jara et al. 2019). Another peak identified was the 2D peak around 2650-2700 cm^{-1}, this indicates presence of graphitic layers (Nicklow, Wakabayashi & Smith 1972).

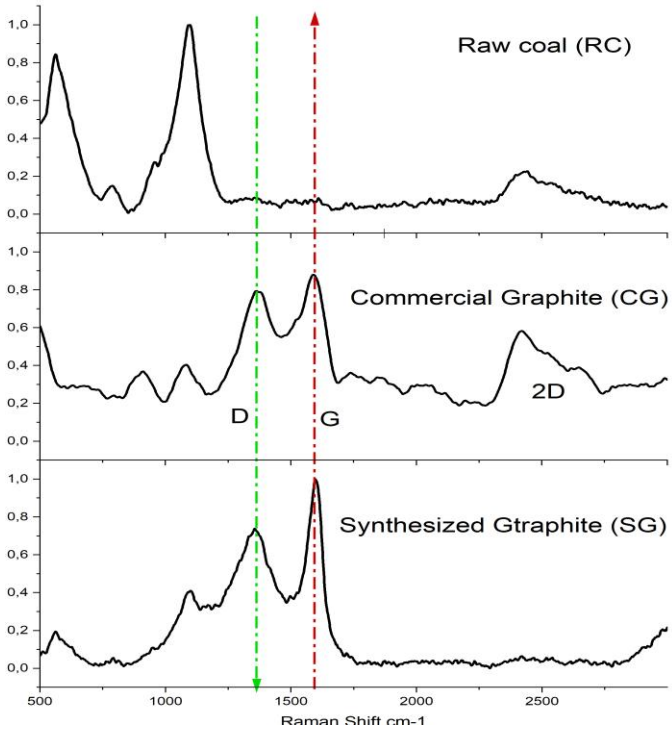

Figure 4.1: Raman spectra of raw coal, commercial graphite and synthesized graphite.

Based on the results obtained, significant differences are observed between the raw coal (RC) sample and the commercial and synthesized graphite (CG & SG). The RC sample exhibits low crystallinity and a highly amorphous nature, as indicated by prominent peaks at 570 cm^{-1} as well as at 1087 cm^{-1}. These peaks are characteristics of disordered carbon structure which is attributed by the structural heterogeneity of raw coal which comprises of organic macerals and inorganic minerals as well as low carbon maturity. The coal sample was classified as low rank sub bituminous coal and hence have not undergone sufficient geological pressure and temperature over time to develop a well ordered crystalline structure hence they retain a significant proportion of aliphatic chains and aromatic clusters . After graphitization, there is a transformation towards polycrystalline graphite in SG, evidenced by the presence of the D peak at 1351 cm^{-1} and G peak at 1593 cm^{-1}. This peaks are indicative of higher crystallinity when compared to RC which lacks long range order due to its heterogeneous organic matrix. The presence of graphitic lamellae in the commercial graphite (CG), used as a reference, is

clearly observed at the peak at 2413 cm^{-1}. Consequently, it is concluded that polycrystalline graphite was synthesized using the metal-assisted microwave method.

Raman spectra bands of RC, CG, and SG were analyzed using curve fitting with Lorenzian subpeaks, as illustrated in Figure *4.2* using Origin2023b software. The D1 band is associated with the primary D peak, while the D2 band usually emerges alongside D1, appearing as a shoulder near the G peak at approximately 1610 cm^{-1}. Its presence tends to decrease as the material's crystallinity improves. (Matthews et al. 1999). The diminishing intensity of the D2 band and the absence of the D3 band as observed from coal to SG indicate the reduction of sp^2-bonded amorphous carbon, oxygenated functional groups, and heterocyclic compounds as coal is subjected to elevated temperatures (Cuesta et al. 1994; Kwiecinska et al. 2010).

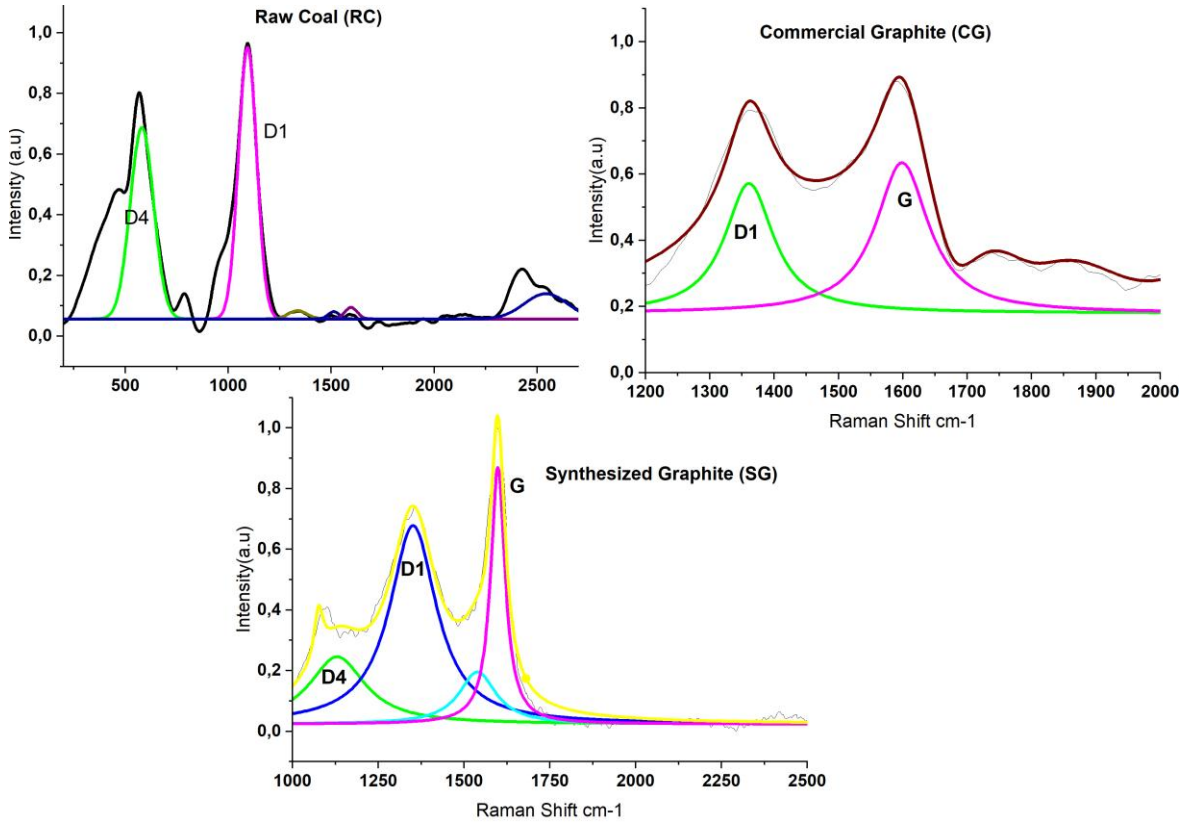

Figure 4.2: Fitted Raman peaks Of Raw coal, Commercial graphite and synthesized graphite.

Structural parameters such as peak intensity, peak area, and the calculated I_D/I_G ratio after peak fitting are summarized in Table 4.2. The ratios I_{D1}/I_G and A_{D1}/A_G are crucial indicators for assessing the degree of graphitization in carbon based materials, with lower values typically reflecting larger graphite microcrystal sizes (Schwan et al., 1996; Pócsik et al., 1998). A lower I_D/I_G is indicative of a higher graphitization and development of a more ordered graphite structure (Khoshk Rish et al., 2021; Hunter, Ramírez-Rico and Schnepp, 2022) . The results presented indicate a decrease in the SG to RC ratio for these parameters, suggesting the formation of more crystalline graphite carbon.

Table 4.2: Parameters from Raman spectroscopy.

Sample	Peak	Position	Peak Intensity	Peak Area	I_{D1}/I_G	A_{D1}/A_G
Raw Coal	D	1337	0,8032	3,11	0,901257	1,083624
	G	1596,57	0,8912	2,87		
Commercial graphite	D	1361,21	0,3318	56,84	0,481358	0,795967
	G	1598,77	0,6893	71,41		
Synthesized Graphite	D	1351,24	0,4702	170,45	0,522619	2,524437
	G	1598,16	0,8997	67,52		

The results suggest that the graphitization of coal was successfully achieved using the metal-assisted microwave method, resulting in significant structural transformation as confirmed by Raman spectroscopy. The R value of the coal sample before graphitization indicates a predominantly disordered structure (Schuepfer et al. 2020). Through the graphitization process of the coal, graphite with a reduced R ratio of 0.52 was synthesized indicating

increased graphitic order and crystallinity (Pócsik et al. 1998; Yuan et al. 2021; Li et al. 2023). This synthesized graphite was compared with commercial graphite available in the market, which showed a slightly lower R value of 0.48. The results showed the effectiveness of the metal-assisted microwave method in producing graphite which has a comparative quality to commercially available material underscoring its potential for industrial applications in carbon materials.

Based on the Raman spectroscopy results, the A_D/A_G ratios obtained were 1.08 for coal, 0.7959 for commercial graphite, and notably higher at 2.52 for synthesized graphite using the metal-assisted microwave method. These ratios are crucial indicators of the degree of graphitization, with higher values typically associated with larger and more ordered graphite microcrystals (Kwiecinska et al. 2010). The A_D/A_G ratio of 1.08 for the initial coal sample indicates a relatively low degree of graphitization, consistent with its predominantly amorphous structure. In contrast, the commercial graphite exhibited a lower A_D/A_G ratio of 0.7959, indicative of a larger crystallite sizes compared to the coal. The synthesized graphite, with an A_D/A_G ratio of 2.52, also demonstrates crystallinity matched to both the coal and the commercial graphite.

These results indicates a successful transformation of coal into polycrystalline graphite through the metal assisted microwave method as shown by the reduction in the I_{D1}/I_G ratio (from 0.90 in RC to 0.52 in SG) and the emergence of sharp D and G bands. This enhanced structural ordering has implications for water treatment applications. The presence of defects sites and residual functional groups in SG enhance adsorption performance by providing active binding sites for pollutants such as heavy metals, dyes, and pharmaceuticals (Datsyuk et al., 2008; Khoshk Rish et al., 2021). The increased crystallinity and thermal stability of SG

also suggest its viability as a precursor for conductive membranes or electrodes in electrochemical water treatment technologies such as capacitive deionization and electro-Fenton processes (Hunter, Ramírez-Rico, & Schnepp, 2022).

The enhanced graphitization of SG contributes to improved mechanical integrity compared to the raw coal precursor. Raw coal, due to its high amorphous content, oxygenated functionalities, and ash impurities, lacks the cohesion and strength necessary for demanding applications. In contrast, SG exhibits an ordered graphitic lamellar structure and reduced disorder, suggesting improved mechanical resilience suitable for membrane fabrication or composite incorporation (Schwan et al., 1996; Pócsik et al., 1998).

4.2.2 FTIR-Infrared Spectroscopy Analysis

The FTIR method was used to pick the functional groups present with in the material (He et al., 2017). As shown in ***Error! Reference source not found.***, the spectra which was processed by baseline correction in the Origin software and fitted with Gaussian functions reveal consistent absorption features across all sample. These includes bands corresponding to aromatic structures (700–900 cm^{-1}), oxygen-containing structure (1000–1800 cm^{-1}), aliphatic C-H stretching (2800–3000 cm^{-1}), and hydroxyl groups (3000–3600 cm^{-1}) (Tian et al., 2016; Yan et al., 2020). A broad O-H stretching vibration peaks appears around 3400 cm^{-1}, indicative of moisture content. However, this peak is not considered in further interpretation due to interference from environmental water absorption and preparation-related factors. Weak peaks at 2925 cm^{-1} and 2850 cm^{-1} were also identified in the spectrum for sample of raw coal (RC), Commercial graphite (CG) and synthesizes graphite (SG), which are ascribed to aliphatic $-CH_2$ and $-CH_3$, respectively. These peaks are more prominent in the raw coal samples and progressively weaken in the CG and SG samples. This reduction in peak intensity suggests graphitization through processes like dehydrogenation

and depolymerization, which are associated with a decrease in aliphatic hydrocarbons (Mukhopadhyay and Gupta, 2012). The dehydrogenation induced by high thermal energy leads to C–H bond dissociation, promoting the formation of more benzene rings in the aromatic structure. This is reflected in the increased intensity of the C=C bond peak around 1635cm^{-1} indicating a higher concentration of C=C bonds as the material undergoes graphitization. The reaction results in the release of hydrogen gas as a by-product.

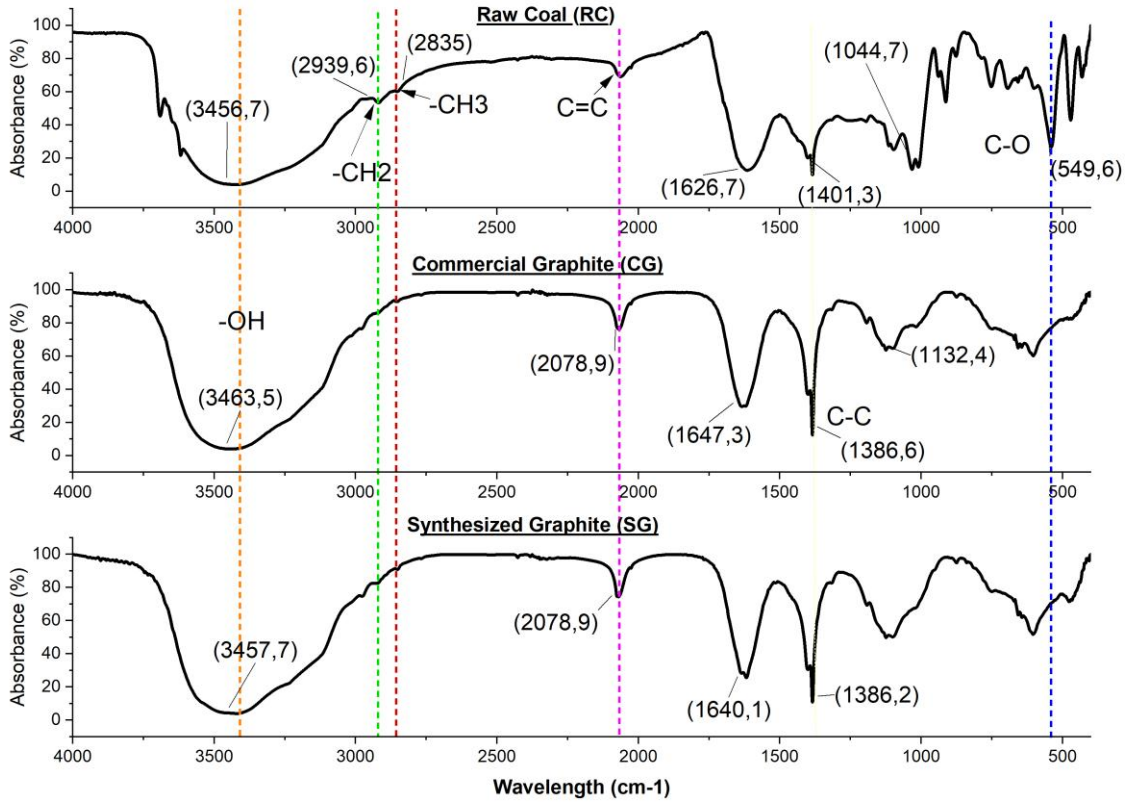

Figure 4.3: The FTIR spectra of Raw coal, commercial coal and synthesized graphite.

Shown in Figure *4.3* shows the decrease in the intensity of oxygenated groups such as C-O at 1385 cm^{-1} with graphitization; therefore, oxygen-containing functional groups engage in the process of aromatic ring condensation. The peaks observed in the range of 700-900 cm^{-1} lie within the FTIR spectrum's fingerprint region (Khoshk Rish et al., 2021) . While these peaks are typically not emphasized, they suggest the presence of aromatic C–H bonds and phenolic

C–O–C deformations (Rodrigues et al., 2011; Qiu et al., 2019; Shi et al., 2021c). These features are attributed to the -CH bending vibrations positioned outside the aromatic system and the contribution of mineral matter. However, there is a convergence of peaks within this area complicates the ability to differentiate specific chemical species.

The FTIR reveals presence of various functional groups in RC which progressively diminish in the synthesized graphite (SG) and commercial graphite (CG) such as hydroxyl (–OH), carbonyl (C=O), and aliphatic C–H groups. In terms of water treatment, the oxygen-containing groups, particularly –OH and –COOH, are known to enhance hydrophilicity, promoting water molecule interactions and improving membrane wettability (Zhao et al., 2014). Therefore, the presence of these groups in RC and partially retained in SG suggests a beneficial surface chemistry for applications requiring water transport, such as in ultrafiltration or adsorptive membrane systems. However, the FTIR results also indicate a reduction of aliphatic and oxygenated groups during graphitization, particularly with the disappearance or weakening of peaks around 2925 cm^{-1} (CH_2) and 1385 cm^{-1} (C–O), reflecting a transition to more aromatic, graphitic structures. While this transformation enhances chemical and thermal stability, it also leads to reduced hydrophilicity (Shi et al., 2021). This trade-off may result in lower initial water flux in membrane applications but can improve long-term durability and resistance to chemical degradation in harsh wastewater environments. Furthermore, the residual oxygenated functionalities in SG, compared to CG, may strike a balance between hydrophilicity and structural integrity, allowing for moderate water affinity and potential adsorption sites for pollutants such as heavy metals and organics (Khoshk Rish et al., 2021).

4.2.3 Morphological Analysis

SEM analysis investigated the morphological features and surface composition of the

samples (Zeng et al., 2022). As shown in the micrographs of Figure *4.4a*, the raw coal sample exhibits an amorphous and irregular morphological structure with compact and blocky particles. The absence of layered structures or defined textures suggests a disordered, non-crystalline carbon matrix, consistent with low rank and limited graphitization. In contrast, Figure *4.4b*, corresponding to CG reveals a flaky, layered structure, characteristics of a well-developed graphitic lamellae. These stacked layers suggest high crystallinity and are indicative of a material with well-aligned sp^2 carbon planes, typical of commercial graphite.

The SEM image in Figure *4.4c*, representing SG displays a partially exfoliated and stacked lamellar structures, effecting the intermediate nature of the material between amorphous coal and fully crystalline graphite. The layered morphology observed in SG indicates successful structural reorganization during metal-assisted microwave treatment, with the formation of graphitic domains and interlayer gaps. These features are beneficial for membrane applications as they support interconnected channels for water transport and provide a pathway for selective permeation of molecules.

Moreover, the rough surface texture and visible micro- and possibly nano-scale porosity across CG and SG samples suggest enhanced surface area and active sites for adsorption. These textural features are advantageous in membrane-based water treatment, particularly for dye removal, where both size exclusion and surface adsorption mechanisms are critical (Zhao et al., 2014; Khoshk Rish et al., 2021). The exfoliated layers can facilitate diffusion of water and pollutants, while the pores contribute to physical entrapment and surface interaction with dye molecules.

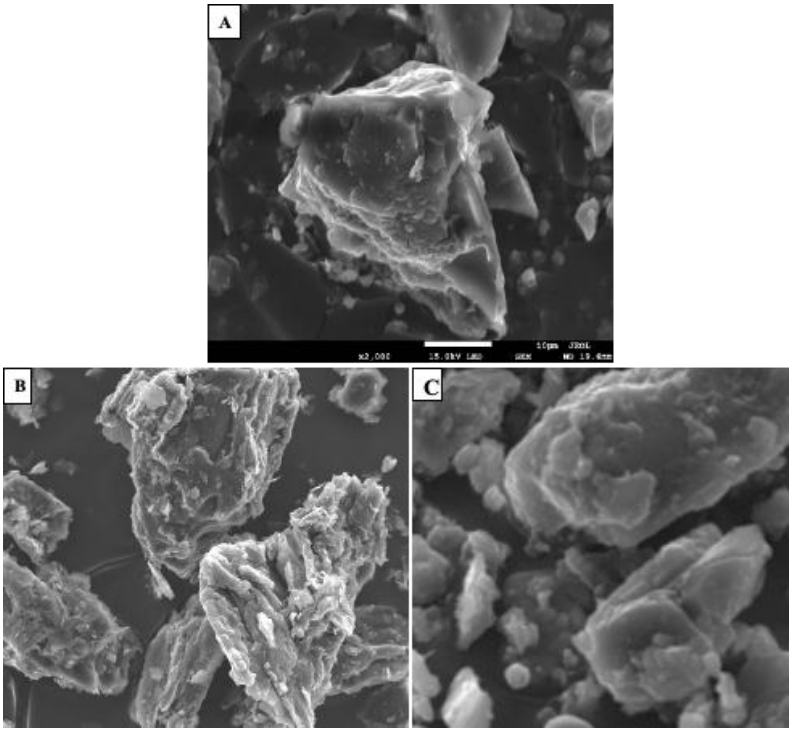

Figure 4.4: Shows the morphology of samples a) raw coal (RC), b) commercial graphite (CG) and c) synthesized graphite (SG) at X2000.

4.3 GO Synthesis

4.3.1 Raman analysis

The Raman spectra of graphene oxide, produced from graphite using various modifications of the Hummers method, are shown in Figure *4.5*. The existence of oxygen functional groups in GO typically induces disorder, which is manifested by the prominent D band observed in the spectra between 1353-1367 cm^{-1} across all samples. Additionally, the spectra exhibit a G band at 1595 cm^{-1}, pointing to the existence of crystalline carbon structures although with varying intensities. According to (Khoshk Rish et al., 2021), the C-C stretching vibrations are indicated by the G band.

The distinct bands observed offers meaningful perspectives on the chemical composition and structural characteristics of the synthesized samples (Khoshk Rish et al., 2021). The T band observed at 1060 cm^{-1}, is associated with the breathing mode of aromatic rings and is

indicative of graphene ordered material (Lockett et al. 2020). This disorder is influenced by presence of oxygen functional groups. The spectra also shows a combined G+D band at 2450 cm^{-1} that is representative to a combination mode of the D and G phonons. This feature is often observed in GO samples (Jin et al. 2021).

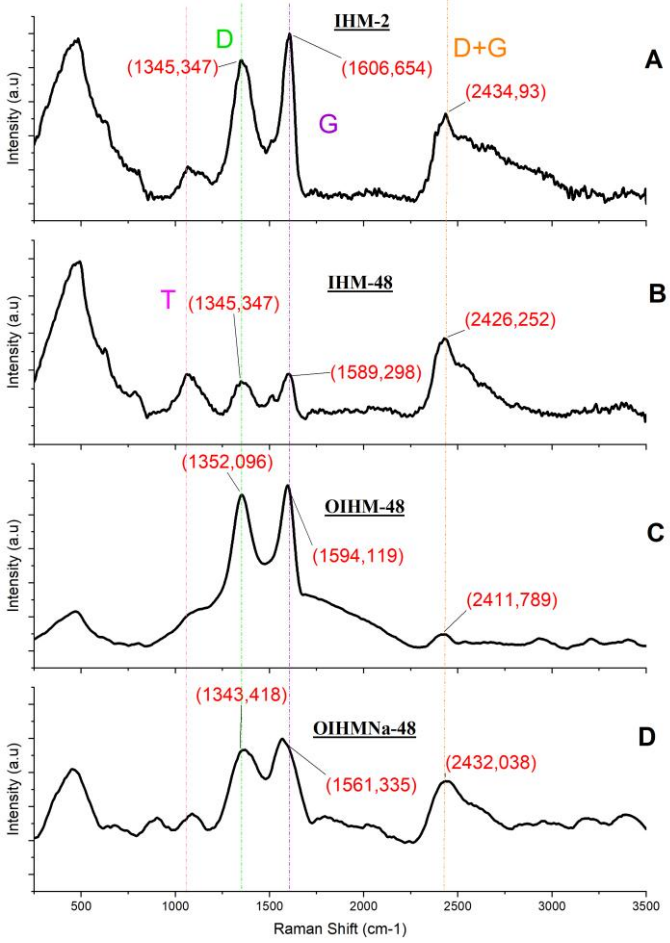

Figure 4.5: Raman spectrums of (a) IHM-2, (b) IHM-48, (c) OIHM-48 and (d) OIHMNa-48.

Following peak fitting, the Raman parameters were obtained, specifically the I_D/I_G ratio as shown in Table *4.3*. This gives important insight into the synthesized graphene oxide samples IHM-2, IHM-48, OIHM-48, and OIHMNa-48. The calculated I_D/I_G ratios were 0.8539, 0.8572, 0.9437, and 0.9153, respectively. These values fall within the typical range of 0.8 to 1.2 as expected for graphene oxide. This ratio assesses the disorder in the carbon structure

with higher ratios suggesting increased structural disorder due to the introduction of oxygen in the graphitic structure (Rabchinskii et al. 2020). The elevated I_D/I_G ratios observed in the synthesized samples confirming the successful introduction of oxygen functionalities through the synthesis activity. This consistency across the samples IHM-2, IHM-48, OIHM-48, and OIHMNa-48 underscores the reliability and reproducibility of the synthesis methods employed.

Table 4.3 Parameters from Raman spectroscopy of GO samples.

Sample	Peak	Position (cm^{-1})	Intensity	I_D/I_G
IHM-2	D	1345	0.8417	0.85391
	G	1606	0.9857	
IHM-48	D	1345	0.3435	0.85725
	G	1589	0.4007	
OIHM-48	D	1352	0.9171	0.94371
	G	1595	0.9718	
OIHMNa-48	D	1343	0.7308	0.91533
	G	1561	0.7984	

4.3.2 FTIR-Infrared Spectroscopy Analysis

Shown in Figure *4.6* is the FTIR analysis of GO samples synthesized through variations of the Hummers' method providing insight into their chemical composition. GO, produced through the oxidation of graphite flakes, was expected to exhibit oxygen functional groups such as carboxyl (-COOH), hydroxyl (-OH), carbonyl (C=O), and ether (C-O-C) (Surekha et al. 2020; Singh 2021). The spectra revealed these distinctive features across the samples. The region between 3700-3400 cm^{-1} prominently displays a high-intensity peak attributed to

hydroxyl groups (-OH), indicative of strong hydrogen bonding interactions. Notably, IHM-48 and OIHMNa-48 exhibit broader -OH peaks, suggesting robust intermolecular interactions, whereas IHM-2 and OIHM-48 display narrower -OH peaks, indicating comparatively weaker interactions.

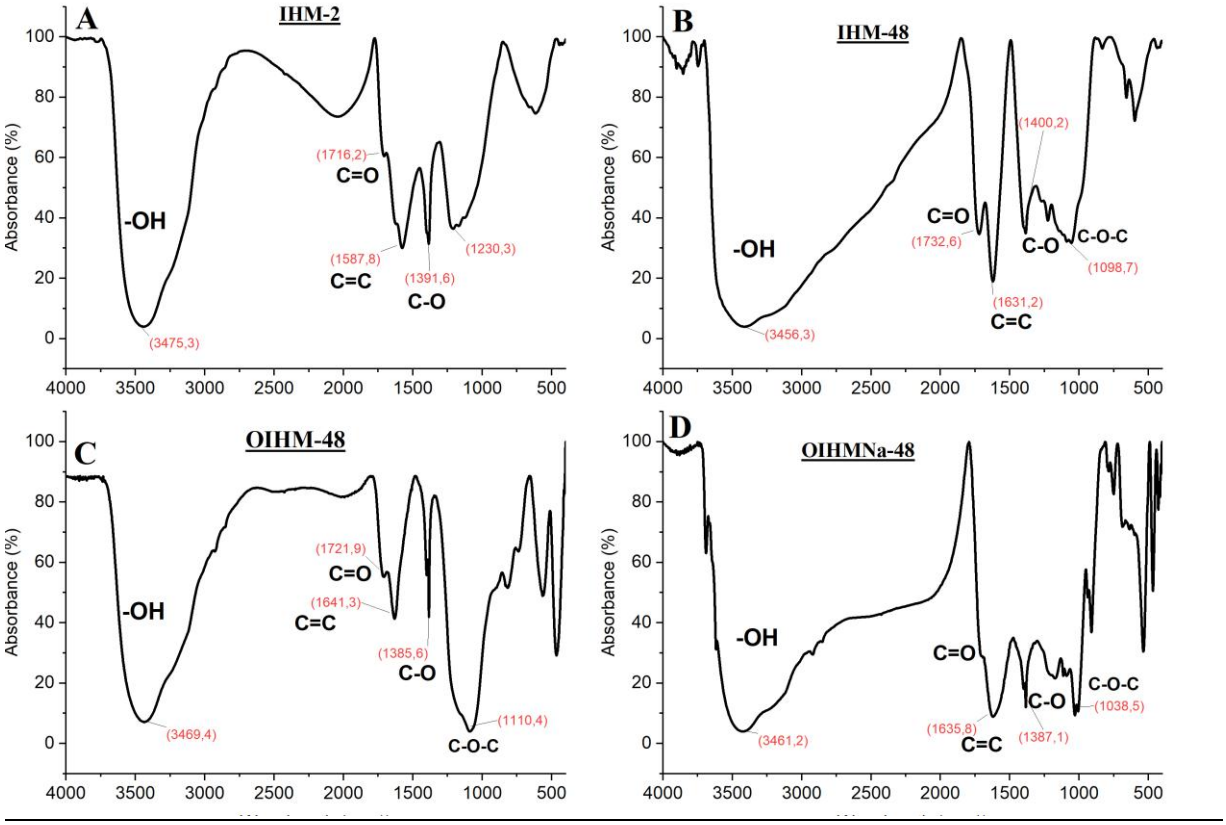

Figure 4.6: FTIR spectra of the samples, highlighting the identified functional groups.

Carbonyl groups (C=O) manifest as intense peaks between 1740-1640 cm^{-1}, with varying intensities observed among the samples. OIHMNa-48 and IHM-48 exhibit a high-intensity peak at 1634 cm^{-1}, whereas OIHM-48 shows a lower intensity at the same wavelength. The presence of C-O functional groups is evident in the 1100-1300 cm^{-1} region, characterized by medium to weak peaks. IHM-48 displays the highest intensity at 1208 cm-1, while IHM-2, OIHM-48, and OIHMNa-48 exhibit points at 1100 cm^{-1}, 1218 cm^{-1}, and 1097 cm^{-1},

respectively. Furthermore, the epoxy C-O-C stretching vibrations are observed in the 500-1000 cm^{-1} range. These are observed at 1038 cm^{-1} for OIHMNa-48, 1097 cm^{-1} for OIHM-48, and 896 cm^{-1} for IHM-2.

The collective presence of carboxylic, hydroxyl, epoxide, and carbonyl groups confirms the substantial oxygenation of both the edge and basal planes of GO (Surekha et al. 2020). This comprehensive analysis substantiates the successful synthesis of GO through the Hummers methods.

4.3.3 Morphological Analysis

The SEM results for the differently fabricated GOs are displayed in Figure *4.7*. What can be observed in all samples is the surface exhibits alterations, including porosity, roughness, and irregularity. The samples exhibit varying degrees of sheet like and crumpled morphologies, consistent with the formation of exfoliated GO structures. Specifically, samples such as IHM-48 and OIHMNa-48 (Figures 4.7b and 4.7d) show layered and wrinkled sheet-like formations, resembling the typical morphology of graphene oxide synthesized via oxidative exfoliation, as reported by Hidayah et al. (2017) and Singh et al. (2016). The crumpled and fibrous textures observed enhance surface area and provide numerous active sites, which are advantageous for adsorption applications including dye removal (Li et al., 2018). These wrinkles and folds are also believed to arise from internal stress during rapid oxidation and exfoliation, which trap functional groups and defects within the layers, improving chemical interaction potential with polar and aromatic dye molecules (Zhou et al., 2013).

Additionally, the porous and flaky appearance in samples like IHM-2 and OIHM-48 (Figures 4.7a and 4.7c) suggests the development of micro and mesoporous structures that are favourable for high water flux and enhanced dye adsorption. The porous texture increases the accessibility of internal surfaces, while the oxygen-containing functional groups confirmed via FTIR and EDS such as carboxyl, hydroxyl, and epoxide groups enhance hydrophilicity

and electrostatic interactions with charged contaminants. These morphological features collectively confirm the success of the oxidation and exfoliation processes applied to coal fines, aligning with similar studies that report increased oxygen functionality and structural disorder in GO synthesized from natural or waste-derived carbon sources (Kolev et al., 2021; Zhang et al., 2019). Overall, the structural characteristics observed in the SEM images are consistent with the findings from Raman and FTIR spectroscopy and underline the material's suitability for water treatment applications such as adsorptive membranes and dye filtration systems.

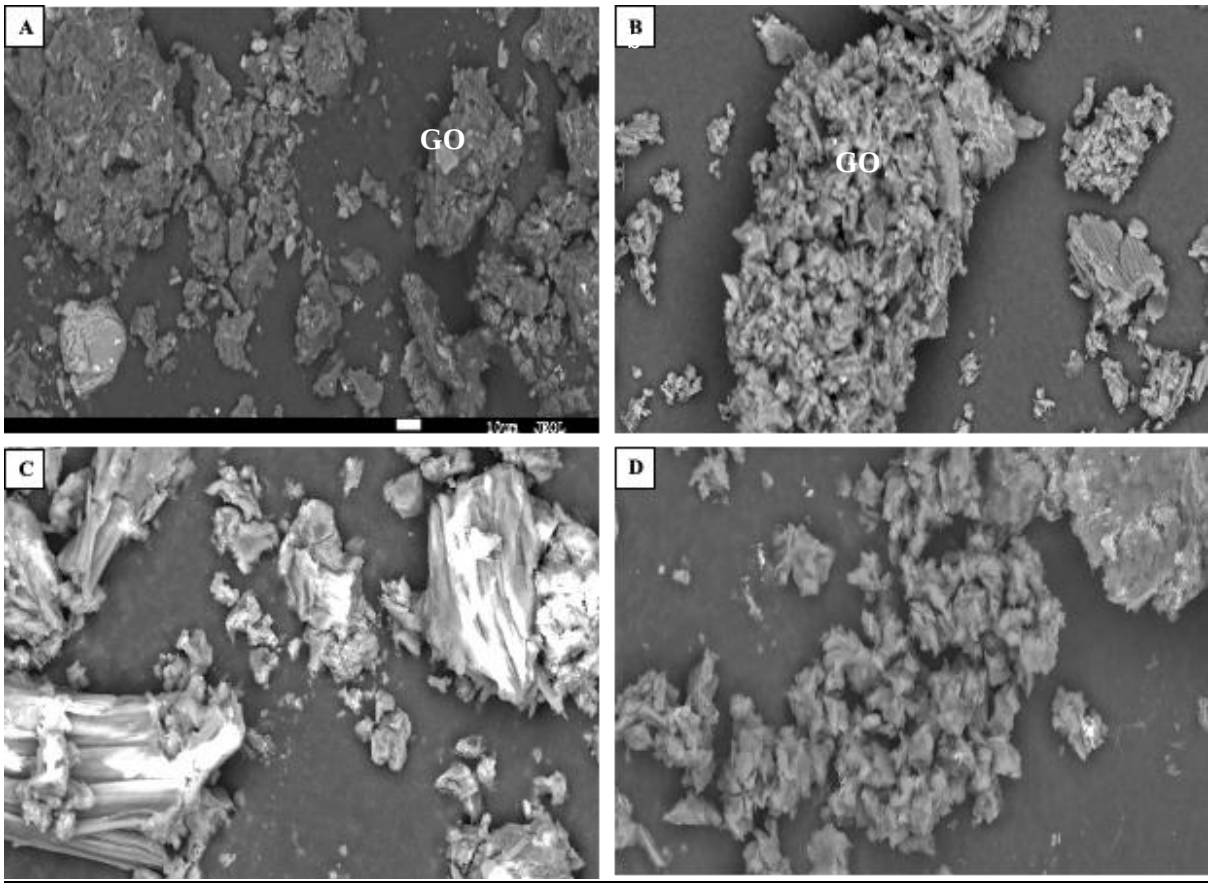

Figure 4.7: SEM micrographs of different coal derived GO (a) IHM-2, (b) IHM-48, (c) OIHM48 and (d) OIHMNa-48, showing exfoliated, wrinkled, and porous morphologies indicative of successful GO synthesis.

The oxidation process was identified using the EDS results shown in Table *4.4*. The weight composition of carbon atoms has decreased when compared to raw coal and synthesized graphite while the oxygen atom composition has increased. The sample with more oxygen atom is OIHM-48. This correlates with the chemical functionalities obtained using the FTIR analysis. The oxidative process that results in GO synthesis from coal structure involves the breaking down of certain bonds in coal such as C-C bonds, C-H bonds, C-O bonds and O-H bonds (Singh, Kumar & Singh 2016; Hidayah et al. 2017; Kolev et al. 2021). The C-C oxidative cleavage results in formation of carboxyl and carbonyl groups while the introduction of Oxygen atoms leads to formation of epoxide groups (Ma et al. 2023). This process facilitates the generation of oxygen-containing functionalities on the carbon surface, increasing the materials oxygen content (Hidayah et al. 2017).

Table 4.4: Shows the percentage weight of Carbon and Oxygen in the sample.

Sample Code	C (%)	O (%)
RC	76.6	8.43
SG	88.4	4.57
IHM-2	67.3	30.1
IHM-48	58.7	38.0
OIHM-48	55.0	40.7
OIHMNa-48	64.2	30.8

4.4 Membrane Analysis Results

4.4.1 Dye rejection and Water flux

The findings reveal that increasing the graphene oxide (GO) concentration enhances methylene blue (MB) rejection for both substrates, though it concurrently reduces the flux Figure *4.8*. Operating with low concentration of 0.05 mg/mL, the membranes showed minimal rejection rates, 3.03% and 5.47% for the two substrates PCB and PAN respectively. This is attributed to the sparse distribution of GO particles located on the surface of the membrane which leads to minimal interaction with the MB dye molecules and hence the low rejection rate and dye capturing as presented in Figure *4.8* (Han et al. 2021; Jia et al. 2022). In contrast, higher rejection was experienced with high GO concentration as there is more GO coverage in the membrane surface. At 0.7 mg/ml concentration, excellent dye rejection was observed for both substrates, which is advocated to the complete coverage of the membranes. This allows for high interaction of the fabricated membrane's MB dye molecules and GO particles, increased membrane tortuosity with an increase in the concentration of GO also results in improved rejection (Jiang et al. 2015; An et al. 2023).

At a 1 mg/mL concentration, membrane clogging occurred for both substrates. This clogging is indicative of the reduced flux associated with higher GO concentrations as shown in Figure *4.9*. Whilst this restrictive layer on the membrane improves dye rejection, it makes it harder for the water to pass through (Kołodziej et al. 2021; Jia et al. 2022). The balance between rejection efficiency and flux is typical in membrane filtration processes. To mitigate the flux reduction, an increase in applied pressure can be used during filtration (You et al. 2018). This pressure helps to overcome the resistance imposed by the restrictive GO layer, therefore allowing more water to pass through the membrane and improving overall filtration efficiency.

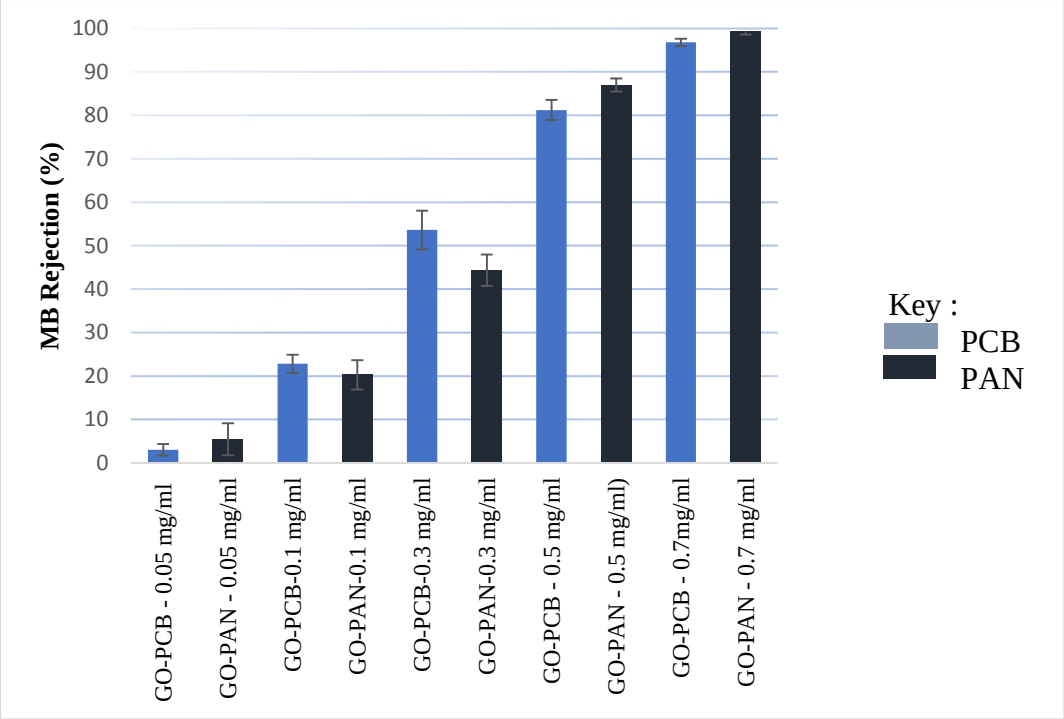

Figure 4.8: Methylene Blue Rejection at Different Concentrations of GO on PCB and PAN Substrates.

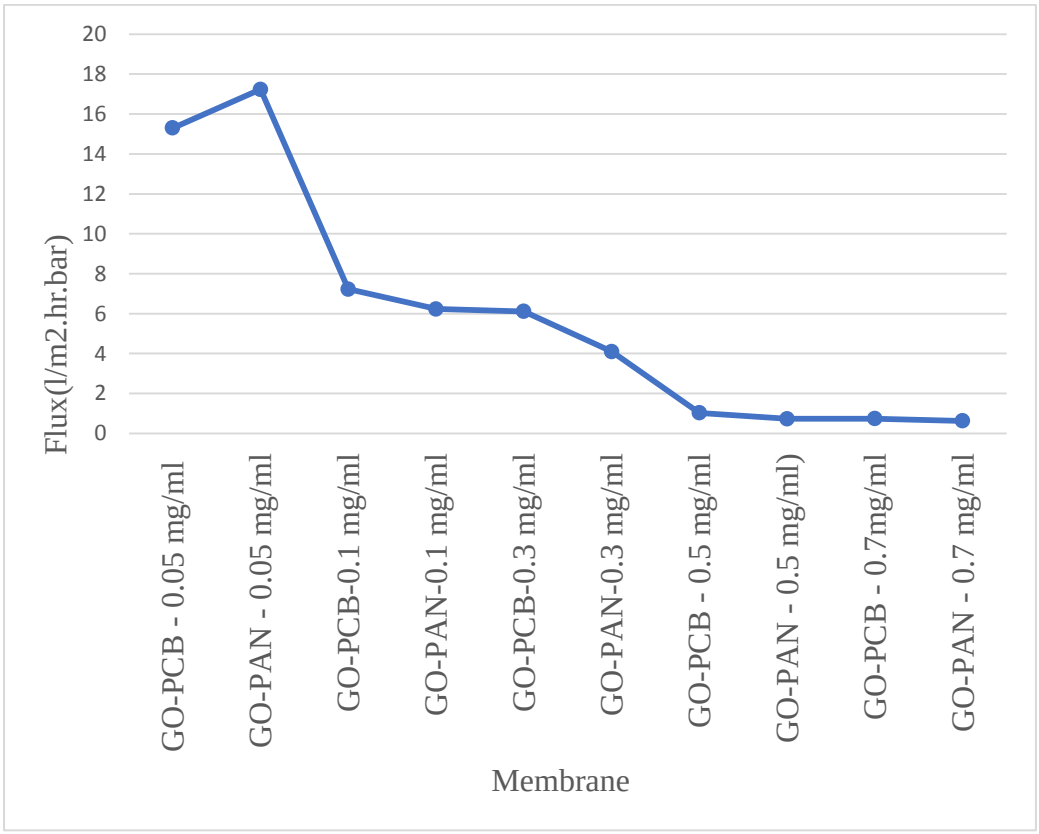

Figure 4.9: Flux performance for different membranes.

An ideal membrane should exhibit high permeate flux, effective rejection, and sufficient mechanical strength to endure the stresses encountered during operation. High permeate flux leads to lower energy consumption and cost. For instance, Hu & Mi (2013) developed a GO membrane exhibiting a high-water flux of 276 $L \cdot m^{-2} \cdot h^{-1} \cdot bar^{-1}$. Similarly, Li et al. (2013) formulated a 3 *n*m GO film that showed an impressive water flux of 1370 $L \cdot m^{-2} \cdot h^{-1} \cdot bar^{-1}$. Wei et al (Wei et al. 2016) prepared membranes of GO using pressure-assisted self-assembly on polysulfon membranes, achieving a water flux range of 3-16 $L \cdot m^{-2} \cdot h^{-1} \cdot bar^{-1}$, along with a rejection rate of 45-72 % for sodium sulfate ($Na_2 SO_4$). Factors such as temperature and degree of oxidation can affect the performance of GO membranes as they affect the chemical properties of GO. In this study, the membrane of GO-PAN (0.05 mg/mL) exhibited a high permeate flux of 15 $L/m^2 \cdot h \cdot bar$, with a rejection rate of 5%. This flux is close to the value obtained by Fan et al. (2020) **,** who attained a permeate flux of 5.44 $L \cdot m^{-2} \cdot h^{-1} \cdot bar^{-1}$ with a membrane made from hydrothermally reduced GO, though their membrane showed a much higher rejection of methylene blue (96.59%).

4.4.2 EWC and Porosity

The EWC and porosity of all fabricated membranes were characterized, and the results are presented in Table *4.5*.EWC refers to the maximum amount of water a hydrophilic membrane can absorb and retain when it reaches a stable state under specific conditions (Zhang et al. 2006a). It was found to increase with the concentration of GO in the membrane, primarily due to the increased mass of GO in the membrane. As the GO concentration increases, its hydrophilicity also increases because of higher accumulation and aggregation of oxygenated functional groups, which in turn enhances water uptake.

Membrane porosity is a key factor influencing the absorption process, as it directly affects both the rejection rate and the membrane permeability flux (Vun et al. 2017). Porosity

measurements were performed only for the best-performing membranes at a concentration of 0.7 mg/mL. The obtained results were found to be 11.2 ± 2.81 % for the GO-PCB membrane and 13.2 ± 1.37 % for the GO-PAN membrane. Since membrane porosity influences permeability, an increase in porosity can enhance permeability, but this often comes at the expense of selectivity due to the larger pore sizes (Zhang et al. 2006b). The results show relatively low porosity values, likely because stacked GO nanosheets introduce significant tortuosity.

Han et al., (Han et al. 2023) used γ-ray irradiation to generate pores and increase in-plane porosity of GO nanosheets, resulting in an optimized membrane with a higher pure water permeability of 345.23 $L \cdot m^{-2} \cdot h^{-1} \cdot bar^{-1}$ and nearly 100 % dye rejection. In a similar study, Rezaee et al., (Rezaee et al. 2015) fabricated a polysulfone-GO membrane for rejection of arsenate in water. The incorporation of GO enhanced the water affinity of the membrane and led to 83.65 % arsenate rejection at 4 bar, exhibiting a pure water flux of 12.5 $L/m^2 \cdot h \cdot bar$. The pure polysulfone membrane had a porosity of 48.3 % and a 25 % rejection rate for arsenate, while the GO membrane showed a porosity of 86.5 % and an arsenate rejection rate of 82 %. Further, Kadhim et al., (Kadhim et al. 2020) demonstrated the porosity of polyethersulfone (PES) membranes could be significantly improved by incorporating GO nanoplates. The control PES membrane had a porosity of 39.92 %, which increased to 80.6% with 0.5 wt% GO. Nonetheless, raising the GO concentration to 1.5 wt % and 2 wt % caused a decrease in porosity, with values of 65.4 % and 67 %, respectively. This pattern is consistent with earlier research indicating that increasing the amount of hydrophilic additives tends to broaden the void spaces and enhance porosity, although an overabundance of GO may actually decrease porosity.

Table 4.5: Characteristics of the fabricated membranes.

Membrane Sample	Hydraulic Resistance (m^2 h/L)	Fouling Resistance (m^2.hr.bar/l)	Equilibrium Water Content (%)	Porosity (%)
GO-PCB – 0.05 mg/ml	29.3±7.77	Not measured	0.15±0.06	Not measured
GO-PAN – 0.05 mg/ml	23.8±8.31	Not measured	0.17±0.09	Not measured
GO-PCB – 0.1 mg/ml	25.6±5.77	Not measured	0.27±0.19	Not measured
GO-PAN – 0.1 mg/ml	19.3±2.43	Not measured	0.24±0.23	Not measured
GO-PCB – 0.3 mg/ml	18.6±6.31	Not measured	0.63±0.17	Not measured
GO-PAN – 0.3 mg/ml	16.4±1.78	Not measured	0.57±0.29	Not measured
GO-PCB – 0.5 mg/ml	12.3±3.31	Not measured	0.87±0.57	Not measured
GO-PAN – 0.5 mg/ml	11.6±3.34	Not measured	0.97±0.73	Not measured
GO-PCB – 0.7 mg/ml	9.6±2.37	0.067±0.48	1.43±0.45	11.2±2.81
GO-PAN – 0.7 mg/ml	7.6±1.34	0.087±0.48	1.57±0.39	13.2±1.37

4.4.3 Membrane hydraulic resistance & fouling resistances

The hydraulic and fouling resistance of GO membranes were analysed at varying concentrations, as illustrated in Table *4.5*. Hydraulic resistance refers to the ease with which water flows through the membrane (Sarihan & Eren 2017). The results indicate a decrease of hydraulic resistance as GO concentration increased reaching as low as 7.6 $m^2 \cdot h/L$ for GO-PAN at 0.7 mg/mL. This is likely due to the dense network of GO sheets, which creates

additional barriers to permeate flow and increases membrane tortuosity, thereby enhancing resistance. Lower resistance suggests higher water permeation potential, however this must be balanced with increasing fouling risk. Over extended use, membrane clogging (especially at > 0.7 mg/mL) may lead to irreversible fouling if not addressed with regular cleaning.

Fouling resistance, on the other hand, pertains to the membrane's ability to resist the attachment of materials on its surface or within its pores during filtration (Rezaee et al. 2015). These fouling interactions can be physical or chemical in nature. Once fouling occurs, it can significantly reduce permeate flux, raise feed pressure, decrease productivity, increase system downtime, elevate maintenance and cleaning costs, and shorten the lifespan of the membrane (Zinadini et al. 2014). During operation, flux is often restored by chemical cleaning. However, this can be expensive and may accelerate membrane degradation.

Fouling resistance was specifically assessed for the best-performing membranes with a 0.7 mg/mL of GO. The fouling resistances of 0.067±0.48 and 0.087±0.48 $m^2 \cdot hr \cdot bar/L$ for the PCB and PAN-based membranes, respectively, which are relatively low, indicating that these membranes are prone to fouling and particle build up. The relatively low fouling resistance values (0.067-0.087 $m^2 \cdot hr \cdot bar/L$) suggest moderate susceptibility to fouling, possibly due to incomplete GO dispersion or surface roughness. The hydrophilic nature of GO improves water interaction, but excess GO can reduce surface smoothness, promoting particulate deposition. Based on the operating environment and membrane composition, organic fouling and particulate fouling are likely dominant. GO's high hydrophilicity typically resists biofouling, but aggregation at high concentrations may result in pore blockage by dye molecules and suspended solids.

Considerable research has been focused on developing antifouling membranes to mitigate the negative impact of fouling on membrane-based separation processes. Materials commonly

used for membrane fabrication such as polyethersulfone (PES), polyvinylidene fluoride (PVDF), and polyacrylonitrile (PAN), are limited in industrial applications due to their low permeation flux and susceptibility to fouling (Al-Maliki et al. 2022). However, a blend of these polymers with GO shows promising results for producing membranes with higher rejection rates and improved antifouling properties. For instance, Xu et al., (Xu et al. 2014) compared PVDF membranes and PVDF-GO composites, finding that the GO-enhanced membranes exhibited superior antifouling performance. Similarly, Zinadini et al., (Zinadini et al. 2014) fabricated PES nanofiltration membranes with GO nanoplates through phase inversion technique. The incorporation of GO significantly improved membrane hydrophilicity, water flux, dye rejection (specifically for direct red), and fouling resistance. The optimal performance was observed with a 0.5 wt.% GO concentration, which provided the best results with respect to water flux, porosity, antifouling properties, and reusability.

5 Chapter 5: CONCLUSION

The thesis primarily focused on leveraging coal stockpiles, accumulated over years of mining, by converting them into graphite, which was subsequently utilized for production of GO. The synthesized graphite, characterized as polycrystalline with a crystallite ratio (R value) of 0.52, which was derived from coal initially possessing a crystallite ratio of 0.90. This transformation represents a notable success, especially when compared to commercial graphite with a crystallite ratio of 0.48.

Furthermore, the GO produced exhibited superior quality, evidenced by a significant increase in the amount of oxygen in the carbon material synthesized. This rose from 8.43% in the raw material to 40.7% when using the OIH48 method. This enhancement underscores the effectiveness of the synthesis process in creating GO of higher purity and functionality, demonstrating its potential for applications such as the efficient in water treatment.

The GO fabricated membranes also showed their efficiency in water treatment as the concentration of GO increased. The experimental study at 0.7mg/mL of GO showed 96.8% and 99.3% MB rejection for GO membrane on PCB and PAN substrates respectively. Therefore, by using the coal fines stockpiles and repurpose into valuable graphene based materials like GO not only addresses the environmental concerns associated with coal fine disposal but also explores innovative solutions for sustainable material utilization.

6 Chapter 6: RECOMMENDATIONS

This chapter entails several recommendations for further exploration drawn from this study to improve the process of coal stockpiles utilization to produce graphite and graphene oxide:

1. It is recommended to do demineralization of coal fines before the graphitization process. This step can potentially enhance the purity and crystallinity of the synthesized graphite and hence improving the properties of the subsequent GO.

2. The use of modified microwave for graphitization can be explored. This technique can allow for precise control over heating rates and temperature therefore minimizing oxidation during the sparking process. It also allows to know the heat produced during sparking by using thermocouples. This approach may lead to the production of graphite with enhanced structural integrity and purity.

3. Comprehensive characterization studies should be conducted to thoroughly evaluate the characteristics of the synthesized GO, such as XPS and TEM for more insight into the structural, chemical, and morphological characteristics.

4. Piloting valuations on the environmental sustainability and economic feasibility of scaling up the production process is crucial. This includes evaluating energy consumption, waste generation, and potential economic benefits associated with utilizing coal stockpiles for graphene production compared to conventional methods.

5. It is recommended to conduct testing using real industrial wastewater sources. This would provide a more realistic assessment of the membrane's performance under complex water matrices containing diverse contaminants. Such validation would offer insights into fouling behaviour, long term stability, and the practical viability of the membrane in real world applications.

REFERENCES

Abd-Elhamid, A.I., Aly, H.F., Soliman, H.A.M. & El-Shanshory, A.A., 2018, 'Graphene oxide: Follow the oxidation mechanism and its application in water treatment', *Journal of Molecular Liquids*, 265.

Agarwal, A., 2017, 'Properties and characteristics of graphite For the', *European University Institute*, (2).

Ajala, O.J., Tijani, J.O., Bankole, M.T. & Abdulkareem, A.S., 2022, 'A critical review on graphene oxide nanostructured material: Properties, Synthesis, characterization and application in water and wastewater treatment', *Environmental Nanotechnology, Monitoring & Management*, 18, 100673.

Alam, S.N., Sharma, N. & Kumar, L., 2017, 'Synthesis of Graphene Oxide (GO) by Modified Hummers Method and Its Thermal Reduction to Obtain Reduced Graphene Oxide (rGO)*', *Graphene*, 06(01).

Ali, I., Basheer, A.A., Mbianda, X.Y., Burakov, A., Galunin, E., Burakova, I., Mkrtchyan, E., Tkachev, A. & Grachev, V., 2019, *Graphene based adsorbents for remediation of noxious pollutants from wastewater*, *Environment International*, 127.

Al-Maliki, R.M., Alsalhy, Q.F., Al-Jubouri, S., Salih, I.K., AbdulRazak, A.A., Shehab, M.A., Németh, Z. & Hernadi, K., 2022, Classification of Nanomaterials and the Effect of Graphene Oxide (GO) and Recently Developed Nanoparticles on the Ultrafiltration Membrane and Their Applications: A Review, Membranes, 12(11).

An, Y.C., Gao, X.X., Jiang, W.L., Han, J.L., Ye, Y., Chen, T.M., Ren, R.Y., Zhang, J.H., Liang, B., Li, Z.L., Wang, A.J. & Ren, N.Q., 2023, A critical review on graphene oxide membrane for industrial wastewater treatment, Environmental Research, 223.

Anawar, H.M., 2015, Sustainable rehabilitation of mining waste and acid mine drainage using geochemistry, mine type, mineralogy, texture, ore extraction and climate knowledge, Journal of Environmental Management, 158.

Arnold, B.J., 2023, 'Coal formation', The Coal Handbook: Volume 1: Towards Cleaner Coal Supply Chains, Second Edition, vol. 1.

ASTM (2013) Standard practice for proximate analysis of coal and coke, ASTM D3172-13. West Conshohocken, PA: ASTM International.

Awan, F.U.R., Arif, M., Iglauer, S. & Keshavarz, A., 2022, 'Coal fines migration: A holistic review of influencing factors', Advances in Colloid and Interface Science, 301, 102595.

Banerjee, A.N., 2018, Graphene and its derivatives as biomedical materials: Future prospects and challenges, Interface Focus, 8(3).

Barnakov, C.N., Khokhlova, G.P., Popova, A.N., Sozinov, S.A. & Ismagilov, Z.R., 2015, 'XRD characterization of the structure of graphites and carbon materials obtained by the low-temperature graphitization of coal tar pitch', Eurasian Chemico-Technological Journal, 17(2).

Borowski, G. & Hycnar, J.J., 2013, 'Utilization of fine coal waste as a fuel briquettes', *International Journal of Coal Preparation and Utilization*, 33(4).

Botha, D.L., Leokaoke, N.T., Bunt, J.R. & Neomagus, H.W.J.P., 2021, 'Evaluation of polymer binders in briquetting of coal fines for combustion applications', *The Journal of the Southern African Institute of Mining and Metallurgy*, 121.

Chen, J., Li, Y., Huang, L., Li, C. & Shi, G., 2015, 'High-yield preparation of graphene oxide from small graphite flakes via an improved Hummers method with a simple purification process', *Carbon*, 81(1), 826–834.

Chen, J., Yao, B., Li, C. & Shi, G., 2013, 'An improved Hummers method for eco-friendly synthesis of graphene oxide', *Carbon*, 64, 225–229.

Chen, X., Qu, Z., Liu, Z. & Ren, G., 2022, 'Mechanism of Oxidization of Graphite to Graphene Oxide by the Hummers Method', *ACS Omega*, 7(27).

Chong, J.Y., Wang, B., Mattevi, C. & Li, K., 2018, 'Dynamic microstructure of graphene oxide membranes and the permeation flux', *Journal of Membrane Science*, 549.

Cuesta, A., Dhamelincourt, P., Laureyns, J., Martínez-Alonso, A. & Tascón, J.M.D., 1994, 'Raman microprobe studies on carbon materials', *Carbon*, 32(8).

Datsyuk, V., Kalyva, M., Papagelis, K., Parthenios, J., Tasis, D., Siokou, A., ... & Galiotis, C. (2008). *Chemical oxidation of multiwalled carbon nanotubes*. Carbon, 46(6), 833–840.

Deng, R., Chu, F., Yu, H., Kwofie, F., Qian, M., Zhou, Y. & Wu, F., 2022, 'Electrochemical performance of expanded graphite prepared from anthracite via a microwave method', *Fuel Processing Technology*, 227, 107100.

Fan, X., Cai, C., Gao, J., Han, X. & Li, J., 2020, 'Hydrothermal reduced graphene oxide membranes for dyes removing', *Separation and Purification Technology*, 241.

Gadekar, M.R. & Ahammed, M.M., 2016, 'Coagulation/flocculation process for dye removal using water treatment residuals: modelling through artificial neural networks', *Desalination and Water Treatment*, 57(55).

Gadekar, M.R. & Ahammed, M.M., 2019, 'Modelling dye removal by adsorption onto water treatment residuals using combined response surface methodology-artificial neural network approach', *Journal of Environmental Management*, 231.

Gao, W., 2015, 'The chemistry of graphene oxide', *Graphene Oxide: Reduction Recipes, Spectroscopy, and Applications*.

Goldstein, J., Newbury, D.E., Joy, D.C., Lyman, C.E., Echlin, P., Lifshin, E., Sawyer, L. and Michael, J.R. (2017) *Scanning electron microscopy and X-ray microanalysis*. 4th edn. New York: Springer.

Gonazález, D., Montes-Morán, M.A., Suárez-Ruiz, I. & Garcia, A.B., 2004, 'Structural characterization of graphite materials prepared from anthracites of different characteristics: A comparative analysis', *Energy and Fuels*, 18(2).

González, D., Montes-Morán, M.A. & Garcia, A.B., 2003, 'Graphite materials prepared from an anthracite: A structural characterization', *Energy and Fuels*, 17(5).

Guo, X., Huan, X. & Chen, X., 2023, 'Feasibility for High-Temperature Graphitization of Deformed Meager Coal', *ACS Omega*, 8(42).

Han, Y., Guo, C., Liu, P., Li, N., Min, C., Zhu, B., Shi, H., Pei, X. & Xu, Z., 2023, 'Graphene oxide membranes with short-range pore channels toward ultrafast water transport via γ-ray etching', *Applied Surface Science*, 608.

Han, Z. yang, Huang, L. jun, Qu, H. jiao, Wang, Yan xin, Zhang, Z. jie, Rong, Q. lin, Sang, Z. qi, Wang, Yao, Kipper, M.J. & Tang, J. guo, 2021, A review of performance improvement strategies for graphene oxide-based and graphene-based membranes in water treatment, *Journal of Materials Science*, 56(16).

He, X., Liu, X., Nie, B. & Song, D., 2017, 'FTIR and Raman spectroscopy characterization of functional groups in various rank coals', *Fuel*, 206.

Hidayah, N.M.S., Liu, W.W., Lai, C.W., Noriman, N.Z., Khe, C.S., Hashim, U. & Lee, H.C., 2017, Comparison on graphite, graphene oxide and reduced graphene oxide: Synthesis and characterization, *AIP Conference Proceedings*, vol. 1892.

Hirsch, A. & Backes, C., 2010, 'Carbon Nanotube Science. Synthesis, Properties and Applications. By Peter J. F. Harris.', *Angewandte Chemie International Edition*, 49(10).

Hu, M. & Mi, B., 2013, 'Enabling graphene oxide nanosheets as water separation membranes', *Environmental Science and Technology*, 47(8).

Hunter, R.D., Ramírez-Rico, J. & Schnepp, Z., 2022, Iron-catalyzed graphitization for the synthesis of nanostructured graphitic carbons, *Journal of Materials Chemistry A*, 10(9).

Islam, F., Tahmasebi, A., Wang, R. & Yu, J., 2021, 'Structure of coal-derived metal-supported few-layer graphene composite materials synthesized using a microwave-assisted catalytic graphitization process', *Nanomaterials*, 11(7).

Jara, A.D., Betemariam, A., Woldetinsae, G. & Kim, J.Y., 2019, Purification, application and current market trend of natural graphite: A review, *International Journal of Mining Science and Technology*, 29(5).

Jia, F., Xiao, X., Nashalian, A., Shen, S., Yang, L., Han, Z., Qu, H., Wang, T., Ye, Z., Zhu, Z., Huang, L., Wang, Y., Tang, J. & Chen, J., 2022, Advances in graphene oxide membranes for water treatment, Nano Research, 15(7).

Jiang, Y., Wang, W.N., Liu, D., Nie, Y., Li, W., Wu, J., Zhang, F., Biswas, P. & Fortner, J.D., 2015, 'Engineered crumpled graphene oxide nanocomposite membrane assemblies for advanced water treatment processes', *Environmental Science and Technology*, 49(11).

Jin, H., Zhu, L., Jin, S., Jiang, L. & Zou, Y., 2021, 'Raman spectroscopy analysis of graphene oxide-enhanced textiles', *Journal of Raman Spectroscopy*, 52(4).

Jovanovski, G., Boev, B. & Makreski, P., 2023, 'Chemistry and geology of coal: nature, composition, coking, gasification, liquefaction, production of chemicals, formation, peatification, coalification, coal types, and ranks', *ChemTexts*, 9(1).

Kadhim, R.J., Al-Ani, F.H., Al-Shaeli, M., Alsalhy, Q.F. & Figoli, A., 2020, 'Removal of dyes using graphene oxide (Go) mixed matrix membranes', *Membranes*, 10(12).

Khan, Z.U., Kausar, A. & Ullah, H., 2016, A Review on Composite Papers of Graphene Oxide, Carbon Nanotube, Polymer/GO, and Polymer/CNT: Processing Strategies, Properties, and Relevance, *Polymer - Plastics Technology and Engineering*, 55(6).

Khoshk Rish, S., Tahmasebi, A., Wang, R., Dou, J. & Yu, J., 2021, 'Formation mechanism of nano graphitic structures during microwave catalytic graphitization of activated carbon', *Diamond and Related Materials*, 120.

Kim, T., Jo, C., Lim, W.G., Lee, Jaegeun, Lee, Jinwoo & Lee, K.H., 2016, 'Facile conversion of activated carbon to battery anode material using microwave graphitization', *Carbon*, 104.

Kolev, S.K., Aleksandrov, H.A., Atanasov, V.A., Popov, V.N. & Milenov, T.I., 2024, 'Surface chemistry of reduced graphene oxide: H-atom transfer reactions', *Applied Surface Science*, 567.

Kołodziej, A., Długoń, E., Świętek, M., Ziąbka, M., Dawiec, E., Gubernat, M., Michalec, M. & Wesełucha-Birczyńska, A., 2021, 'A raman spectroscopic analysis of polymer membranes with graphene oxide and reduced graphene oxide', *Journal of Composites Science*, 5(1).

Krishnan, D., Raidongia, K., Shao, J. & Huang, J., 2014, 'Graphene oxide assisted hydrothermal carbonization of carbon hydrates', *ACS Nano*, 8(1).

Kumari, T.S.D., 2020, Catalytic graphitization: A bottom-up approach to graphene and quantum dots derived therefrom-A review, *Materials Today: Proceedings*, vol. 46.

Kusrini, E., Santoso, E. and Wahyudi, S.T., 2018. Evaluation of Indonesian low-rank coal properties for combustion applications. *International Journal of Energy Research*, 42(10).

Kwiecinska, B., Suárez-Ruiz, I., Paluszkiewicz, C. & Rodriques, S., 2010, 'Raman spectroscopy of selected carbonaceous samples', *International Journal of Coal Geology*, 84(3–4).

Lacina, K., Kubesa, O., Horáčková, V., Moravec, Z., Kuta, J., Vanýsek, P. & Skládal, P., 2018, 'Graphene Oxide from Improved Hummers' Method: Is This Material Suitable for Reproducible Electrochemical (Bio)Sensing?', *ECS Journal of Solid State Science and Technology*, 7(10).

Lerf, A., He, H., Forster, M. & Klinowski, J., 1998, 'Structure of graphite oxide revisited', *Journal of Physical Chemistry B*, 102(23).

Li, H., Song, Z., Zhang, X., Huang, Y., Li, S., Mao, Y., Ploehn, H.J., Bao, Y. & Yu, M., 2013, 'Ultrathin, molecular-sieving graphene oxide membranes for selective hydrogen separation', *Science*, 342(6154).

Li, J., Qin, Y., Chen, Y., Shen, J., Song, Y. & Wang, Z., 2023, 'Structural characteristics and evolution of meta-anthracite to coaly graphite: A quantitative investigation using X-ray diffraction, Raman spectroscopy, and high-resolution transmission electron microscopy', *Fuel*, 333.

Li, K., Liu, Q., Cheng, H., Hu, M. & Zhang, S., 2021, 'Classification and carbon structural transformation from anthracite to natural coaly graphite by XRD, Raman spectroscopy, and HRTEM', *Spectrochimica Acta - Part A: Molecular and Biomolecular Spectroscopy*, 249.

Li, K., Rimmer, S.M., Liu, Q. & Zhang, Y., 2019, 'Micro-Raman Spectroscopy of Microscopically Distinguishable Components of Naturally Graphitized Coals from Central Hunan Province, China', *Energy and Fuels*, 33(2).

Li, Q., Jiang, J., Zhang, Q., Zhou, W., Cai, S., Duan, L., Ge, S. & Hao, J., 2016, 'Influences of coal size, volatile matter content, and additive on primary particulate matter emissions from household stove combustion', *Fuel*, 182.

Li, Y., Tian, X., Song, Y., Yang, T., Wu, S. & Liu, Z., 2022, 'Preparation and lithium storage of anthracite-based graphite anode materials', New Carbon Materials, 37(6).

Liu, Y., 2017, Application of graphene oxide in water treatment, *IOP Conference Series: Earth and Environmental Science*, vol. 94.

Lockett, M., Sarmiento, V., Balingit, M., Oropeza-Guzmán, M.T. & Vázquez-Mena, O., 2020, 'Direct chemical conversion of continuous CVD graphene/graphite films to graphene oxide without exfoliation', *Carbon*, 158.

Lv, X., Zhang, T., Luo, Y., Zhang, Y., Wang, Y. & Zhang, G., 2020, 'Study on carbon nanotubes and activated carbon hybrids by pyrolysis of coal', *Journal of Analytical and Applied Pyrolysis*, 146.

Lyu, J., Wen, X., Kumar, U., You, Y., Chen, V. & Joshi, R.K., 2018, Separation and purification using GO and r-GO membranes, *RSC Advances*, 8(41).

Ma, J., Ping, D. & Dong, X., 2017, Recent developments of graphene oxide-based membranes: A review, *Membranes*, 7(3).

Ma, J., Tang, X., He, Y., Fan, Y., Chen, J. & HaoYu, 2020, 'Robust stable MoS2/GO filtration membrane for effective removal of dyes and salts from water with enhanced permeability', *Desalination*, 480.

Ma, L., Wu, Y., Lin, J., Jiang, H., Zhang, Y., Chen, X. and Zhang, X., 2023. The influence of oxygen-containing functional groups on the physicochemical properties of activated carbon: insights from XPS and TPD. *Coatings*, 13(4), p.654

Manoj, B., 2020, 'Synthesis of Coal-based Nanocarbon Advances and Applications', *Pure and Functionalized Carbon Based Nanomaterials*.

Marcano, D.C., Kosynkin, D. V., Berlin, J.M., Sinitskii, A., Sun, Z., Slesarev, A.S., Alemany, L.B., Lu, W. & Tour, J.M., 2018, 'Correction to Improved Synthesis of Graphene Oxide', *ACS Nano*, 12(2).

Masi, C.A., Schumacher, T.A., Hilman, J., Dulal, R., Rimal, G., Xu, B., Leonard, B., Tang, J., Fan, M. & Chien, T.Y., 2021, 'Converting raw coal powder into polycrystalline nano-graphite by metal-assisted microwave treatment', *Nano-Structures & Nano-Objects*, 25, 100660.

Massaro, M.M., Son, S.F. & Groven, L.J., 2024, 'Mechanical, pyrolysis, and combustion characterization of briquetted coal fines with municipal solid waste plastic (MSW) binders', *Fuel*, 115.

Matthews, M.J., Pimenta, M.A., Dresselhaus, G., Dresselhaus, M.S. & Endo, M., 1999, 'Origin of dispersive effects of the Raman D band in carbon materials', *Physical Review B - Condensed Matter and Materials Physics*, 59(10).

Medupe, A., Muzenda, E., Rapoo, M., Nkosi, N. & Gorimbo, J., 2019, Pyrolysis of Morupule Coal Dust for the Production of Tar, Proceedings of 2019 7th International Renewable and Sustainable Energy Conference, IRSEC 2019.

Moolman, D., Falcon, R.M.S. and Waanders, F.B**.,** 2019. Petrological and geochemical properties of South African coals with high ash content. *Journal of African Earth Sciences*, 152

MOOSA, A.A. & ABED, M.S., 2021, Graphene preparation and graphite exfoliation, Turkish *Journal of Chemistry*, 45(3).

Mouhat, F., Coudert, F.X. & Bocquet, M.L., 2020, 'Structure and chemistry of graphene oxide in liquid water from first principles', *Nature Communications*, 11(1).

Mukhopadhyay, P. & Gupta, R.K., 2012, Graphite, graphene, and their polymer nanocomposites.

Nicklow, R., Wakabayashi, N. & Smith, H.G., 1972, 'Lattice dynamics of pyrolytic graphite', *Physical Review B*, 5(12).

Ning, X. jun, Liang, W., Zhang, J. liang, Wang, G. wei, Li, Y. jiang & Jiang, C. he, 2019, 'Effect of ash on coal structure and combustibility', *International Journal of Minerals, Metallurgy and Materials*, 26(8).

Omoriyekomwan, J.E., Tahmasebi, A., Zhang, J. & Yu, J., 2019, 'Mechanistic study on direct synthesis of carbon nanotubes from cellulose by means of microwave pyrolysis', *Energy Conversion and Management*, 192.

Orem, W.H. & Finkelman, R.B., 2013, 'Coal Formation and Geochemistry', *Treatise on Geochemistry: Second Edition*, vol. 9.

Pavia, D.L., Lampman, G.M., Kriz, G.S. and Vyvyan, J.R. (2015) Introduction to spectroscopy. 5th edn. Boston, MA: Cengage Learning.

Perera, F.P., 2017, Multiple threats to child health from fossil fuel combustion: Impacts of air pollution and climate change, Environmental Health Perspectives, 125(2).

Plachá, D. & Jampilek, J., 2019, *Graphenic materials for biomedical applications*, *Nanomaterials*, 9(12).

Pócsik, I., Hundhausen, M., Koós, M. & Ley, L., 1998, 'Origin of the D peak in the Raman spectrum of microcrystalline graphite', *Journal of Non-Crystalline Solids*, 227–230(PART 2).

Prakash, J., 2022, Mechanistic Insights into Graphene Oxide Driven Photocatalysis as Co-Catalyst and Sole Catalyst in Degradation of Organic Dye Pollutants, *Photochem*, 2(3).

Purwandari, V., Gea, S., Wirjosentono, B. & Haryono, A., 2018, Synthesis of graphene oxide from the Sawahlunto-Sijunjung coal via modified hummers method, *AIP Conference Proceedings*, vol. 2049.

Qiu, C., Liu, D., Jin, K., Fang, L., Xie, G. & Robertson, J., 2017, 'Electrochemical functionalization of 316 stainless steel with polyaniline-graphene oxide: Corrosion resistance study', *Materials Chemistry and Physics*, 198.

Qiu, T., Yang, J.G. & Bai, X.J., 2020, 'Preparation of coal-based graphite with different microstructures by adjusting the content of ash and volatile matter in raw coal', *Energy Sources, Part A: Recovery, Utilization and Environmental Effects*, 42(15).

Qiu, T., Yang, J.G., Bai, X.J. & Wang, Y.L., 2019, 'The preparation of synthetic graphite materials with hierarchical pores from lignite by one-step impregnation and their characterization as dye absorbents', *RSC Advances*, 9(22).

Rabchinskii, M.K., Ryzhkov, S.A., Kirilenko, D.A., Ulin, N. V., Baidakova, M. V., Shnitov, V. V., Pavlov, S.I., Chumakov, R.G., Stolyarova, D.Y., Besedina, N.A., Shvidchenko, A. V., Potorochin, D. V., Roth, F., Smirnov, D.A., Gudkov, M. V., Brzhezinskaya, M., Lebedev, O.I., Melnikov, V.P. & Brunkov, P.N., 2020, 'From graphene oxide towards aminated graphene: facile synthesis, its structure and electronic properties', *Scientific Reports*, 10(1).

Rajakumar, G., Zhang, X.H., Gomathi, T., Wang, S.F., Ansari, M.A., Mydhili, G., Nirmala, G., Alzohairy, M.A. & Chung, I.M., 2020, Current use of carbon-based materials for biomedical applications-A prospective and review, *Processes*, 8(3).

Rath, L.K., Tripathy, A. and Singh, V.K**.,** 2014. Characterization and washability studies of Indian thermal coals. *International Journal of Coal Preparation and Utilization*, 34(4), pp.173–185.

Razaq, A., Bibi, F., Zheng, X., Papadakis, R., Jafri, S.H.M. & Li, H., 2022, Review on Graphene-, Graphene Oxide-, Reduced Graphene Oxide-Based Flexible Composites: From Fabrication to Applications, *Materials*, 15(3).

Rezaee, R., Nasseri, S., Mahvi, A.H., Nabizadeh, R., Mousavi, S.A., Rashidi, A., Jafari, A. & Nazmara, S., 2015, 'Fabrication and characterization of a polysulfone-graphene oxide nanocomposite membrane for arsenate rejection from water', *Journal of Environmental Health Science and Engineering*, 13(1).

Rodrigues, S., Suárez-Ruiz, I., Marques, M., Flores, D., Camean, I. & García, A.B., 2011, 'Development of graphite-like particles from the high temperature treatment of carbonized anthracites', *International Journal of Coal Geology*, 85(2).

Sahoo, P.C., Dash, T., Mallick, S.C., Mohanty, N. & Biswal, S.K., 2024, 'A study on graphene oxide and its nanocomposites: preparation, properties and applications in water and wastewater treatment', *Comprehensive Analytical Chemistry*.

Sarihan, A. & Eren, E., 2017, 'Novel high performanced and fouling resistant PSf/ZnO membranes for water treatment', *Membrane Water Treatment*, 8(6).

Schuepfer, D.B., Badaczewski, F., Guerra-Castro, J.M., Hofmann, D.M., Heiliger, C., Smarsly, B. & Klar, P.J., 2020, 'Assessing the structural properties of graphitic and non-graphitic carbons by Raman spectroscopy', *Carbon*, 161.

Schwan, J., Ulrich, S., Batori, V., Ehrhardt, H. & Silva, S.R.P., 1996, 'Raman spectroscopy on amorphous carbon films', *Journal of Applied Physics*, 80(1).

Shi, M., Song, C., Tai, Z., Zou, K., Duan, Y., Dai, X., Sun, J., Chen, Y. & Liu, Y., 2021, 'Coal-derived synthetic graphite with high specific capacity and excellent cyclic stability as anode material for lithium-ion batteries', *Fuel*, 292, 120250.

Singh, P.K., 2021, 'Thermo Gravimetric Analysis and FTIR Analysis of Electrochemically Synthesized Graphene Oxide (GO)/Reduced Graphene Oxide (rGO)', *IOP Conference Series: Materials Science and Engineering*, 1116(1).

Singh, R.K., Kumar, R. & Singh, D.P., 2016, 'Graphene oxide: strategies for synthesis, reduction and frontier applications'.

Singh, S.B., Haskin, N. & Dastgheib, S.A., 2023, Coal-based graphene oxide-like materials: A comprehensive review, *Carbon*, 215.

Smith, A.T., LaChance, A.M., Zeng, S., Liu, B. & Sun, L., 2019a, 'Synthesis, properties, and applications of graphene oxide/reduced graphene oxide and their nanocomposites', *Nano Materials Science*, 1(1), 31–47.

Sohail, M., Saleem, M., Ullah, S., Saeed, N., Afridi, A., Khan, M. & Arif, M., 2017, 'Modified and improved Hummer's synthesis of graphene oxide for capacitors applications', *Modern Electronic Materials*, 3(3), 110–116.

Speight, J. G., 2013. The Chemistry and Technology of Coal (3rd ed.). CRC Press.

Stonestreet, P. & Franzidis, J.P., 1988, 'Reverse flotation of coal—A novel way for the beneficiation of coal fines', *Minerals Engineering*, 1(4), 343–349.

Sun, L., 2019, Structure and synthesis of graphene oxide, *Chinese Journal of Chemical Engineering*, 27(10).

Surekha, G., Krishnaiah, K.V., Ravi, N. & Padma Suvarna, R., 2020, FTIR, Raman and XRD analysis of graphene oxide films prepared by modified Hummers method, *Journal of Physics: Conference Series*, vol. 1495.

Tamuly, J., Bhattacharjya, D. & Saikia, B.K., 2022, Graphene/Graphene Derivatives from Coal, Biomass, and Wastes: Synthesis, Energy Applications, and Perspectives, *Energy and Fuels*, 36(21).

Tang, L., Mao, Q., You, Z., Yao, Z., Zhu, X., Zhong, Q. & Xiao, J., 2022, 'Catalytic graphitization in anthracite by reduced iron particles and investigating the mechanism of catalytic transformation via molecular dynamics', *Carbon*, 188.

Tang, Y., Chen, P., Li, R., Huan, X., Xu, J., Fan, J. & Che, Q., 2021, 'Model construction and optimization of molecule structure of coal-based grapheme oxide from Jingxi coal', *Meitan Kexue Jishu/Coal Science and Technology (Peking)*, 49(6).

Tian, B., Qiao, Y.Y., Tian, Y.Y. & Liu, Q., 2016, 'Investigation on the effect of particle size and heating rate on pyrolysis characteristics of a bituminous coal by TG-FTIR', *Journal of Analytical and Applied Pyrolysis*, 121.

Totton, T.S., Misquitta, A.J. & Kraft, M., 2011, 'Assessing the polycyclic aromatic hydrocarbon anisotropic potential with application to the exfoliation energy of graphite', *Journal of Physical Chemistry A*, 115(46).

Urade, A.R., Lahiri, I. & Suresh, K.S., 2023, *Graphene Properties, Synthesis and Applications: A Review*, *JOM*, 75(3).

Vun, C.P., Mohammad, A.W., Haan, T.Y. & Mahmoudi, E., 2017, 'Evaluation of Iron oxide decorated on graphene oxide (FE3O4/GO) nanohybrid incorporated in PSF membrane at different molar ratios for Congo red rejection', *Jurnal Teknologi*, 79(1–2).

Wang, L., Qiu, T., Guo, Z., Shen, X., Yang, J. & Wang, Y., 2021, 'Changes and Migration of Coal-Derived Minerals on the Graphitization Process of Anthracite', *ACS Omega*, 6(1).

Wang, T., Wang, Y., Cheng, G., Ma, C., Liu, X., Wang, J., Qiao, W. & Ling, L., 2020, 'Catalytic Graphitization of Anthracite as an Anode for Lithium-Ion Batteries', *Energy and Fuels*, 34(7).

Wei, N., Peng, X. & Xu, Z., 2014, 'Understanding water permeation in graphene oxide membranes', *ACS Applied Materials and Interfaces*, 6(8).

Wei, Y., Zhang, Y., Gao, X., Yuan, Y., Su, B. & Gao, C., 2016, 'Declining flux and narrowing nanochannels under wrinkles of compacted graphene oxide nanofiltration membranes', *Carbon*, 108.

Xia, W., Yang, J. & Liang, C., 2014, 'Investigation of changes in surface properties of bituminous coal during natural weathering processes by XPS and SEM', *Applied Surface Science*, 293.

Xia, Z.Y., Pezzini, S., Treossi, E., Giambastiani, G., Corticelli, F., Morandi, V., Zanelli, A., Bellani, V. & Palermo, V., 2013, 'The exfoliation of graphene in liquids by electrochemical, chemical, and sonication-assisted techniques: A nanoscale study', *Advanced Functional Materials*, 23(37).

Xing, B., Zhang, Chuantao, Cao, Y., Huang, G., Liu, Q., Zhang, Chuanxiang, Chen, Z., Yi, G., Chen, L. & Yu, J., 2018, 'Preparation of synthetic graphite from bituminous coal as anode materials for high performance lithium-ion batteries', *Fuel Processing Technology*, 172.

Xu, Z., Zhang, J., Shan, M., Li, Y., Li, B., Niu, J., Zhou, B. & Qian, X., 2014, 'Organosilane-functionalized graphene oxide for enhanced antifouling and mechanical properties of polyvinylidene fluoride ultrafiltration membranes', *Journal of Membrane Science*, 458.

Yadav, N. & Lochab, B., 2019, 'A comparative study of graphene oxide: Hummers, intermediate and improved method', *FlatChem*, 13, 40–49.

Yan, J., Lei, Z., Li, Z., Wang, Z., Ren, S., Kang, S., Wang, X. & Shui, H., 2020, 'Molecular structure characterization of low-medium rank coals via XRD, solid state 13C NMR and FTIR spectroscopy', *Fuel*, 268.

Yang, G., Zhang, D., Zhu, G., Zhou, T., Song, M., Qu, L., Xiong, K. & Li, H., 2020, 'A Sm-MOF/GO nanocomposite membrane for efficient organic dye removal from wastewater', *RSC Advances*, 10(14).

Yang, L., Jia, F., Juan, Z., Yu, D., Sun, L., Wang, Y., Huang, L. & Tang, J., 2022, 'Bioinspired graphene oxide nanofiltration membranes with ultrafast water transport and selectivity for water treatment', *FlatChem*, 36, 100450.

Yi, L., Feng, J., Qin, Y.H. & Li, W.Y., 2017, 'Prediction of elemental composition of coal using proximate analysis', *Fuel*, 193.

You, Y., Jin, X.H., Wen, X.Y., Sahajwalla, V., Chen, V., Bustamante, H. & Joshi, R.K., 2018, 'Application of graphene oxide membranes for removal of natural organic matter from water', *Carbon*, 129.

Yuan, L., Liu, Q., Mathews, J.P., Zhang, H. & Wu, Y., 2021, 'Quantifying the Structural Transitions of Chinese Coal to Coal-Derived Natural Graphite by XRD, Raman Spectroscopy, and HRTEM Image Analyses', *Energy and Fuels*, 35(3).

Zaaba, N.I., Foo, K.L., Hashim, U., Tan, S.J., Liu, W.W. & Voon, C.H., 2017, 'Synthesis of Graphene Oxide using Modified Hummers Method: Solvent Influence', *Procedia Engineering*, 184, 469–477.

Zeng, L., Wang, Y., Guo, Y., Dai, X., Chen, L., He, C., Nhung, N.T.H., Wei, Y., Dodbiba, G. & Fujita, T., 2022, 'Improved Method for Preparing Nanospheres from Pomelo Peel to Achieve High Graphitization at a Low Temperature', *Crystals*, 12(3).

Zhang, T., Wang, Q., Li, G., Zhao, Y., Lv, X., Luo, Y. & Zhang, Y., 2019, 'Formation of carbon nanotubes from potassium catalyzed pyrolysis of bituminous coal', *Fuel*, 239.

Zhang, X., Wang, S., Chen, H., Wang, X., Deng, J., Li, X. & Zhang, Y., 2023, 'Observation of carbon nanostructure and evolution of chemical structure from coal to graphite by high temperature treatment, using componential determination, X-ray diffraction and high-resolution transmission electron microscope', *Fuel*, 332.

Zhang, Z., Gao, J., Zhang, W. & Ren, Z., 2006a, 'Experimental study of the effect of membrane porosity on membrane absorption process', *Separation Science and Technology*, 41(14).

Zhang, Z., Gao, J., Zhang, W. & Ren, Z., 2006b, 'Experimental study of the effect of membrane porosity on membrane absorption process', *Separation Science and Technology*, 41(14).

Zhuo, Y., Xie, Z. & Shen, Y., 2021, 'Model study of carbonisation of low rank coal briquettes: Effect of briquettes shape', *Powder Technology*, 385.

Zinadini, S., Zinatizadeh, A.A., Rahimi, M., Vatanpour, V. & Zangeneh, H., 2014, 'Preparation of a novel antifouling mixed matrix PES membrane by embedding graphene oxide nanoplates', *Journal of Membrane Science*, 453.

1859, 'XIII. On the atomic weight of graphite', *Philosophical Transactions of the Royal Society of London*, 149.

APPENDIX

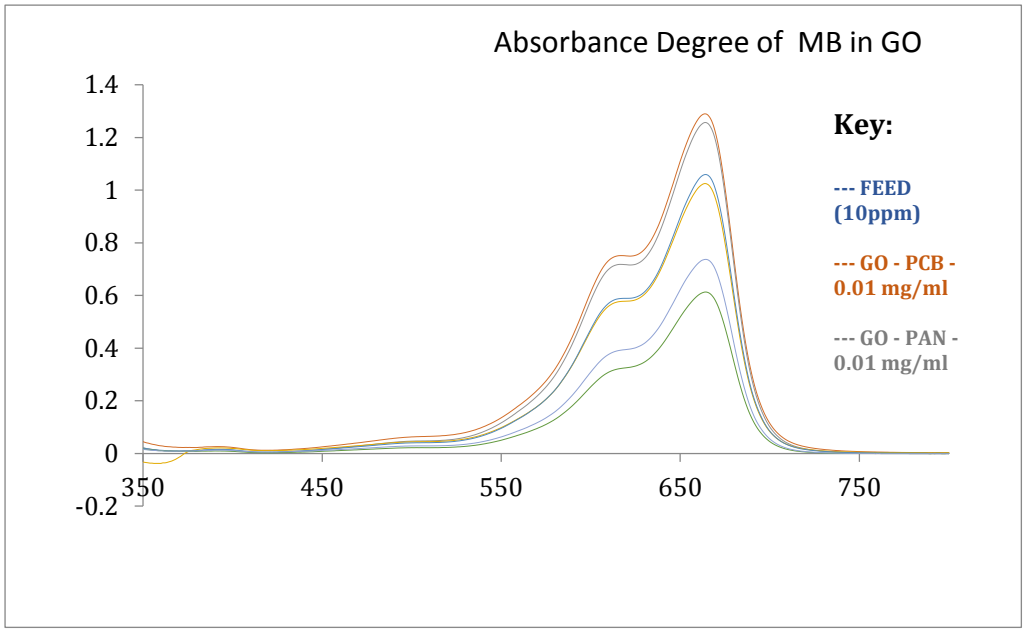

Figure A1: Absorbance Degree of Methylene Blue in GO Membrane at low concentrations

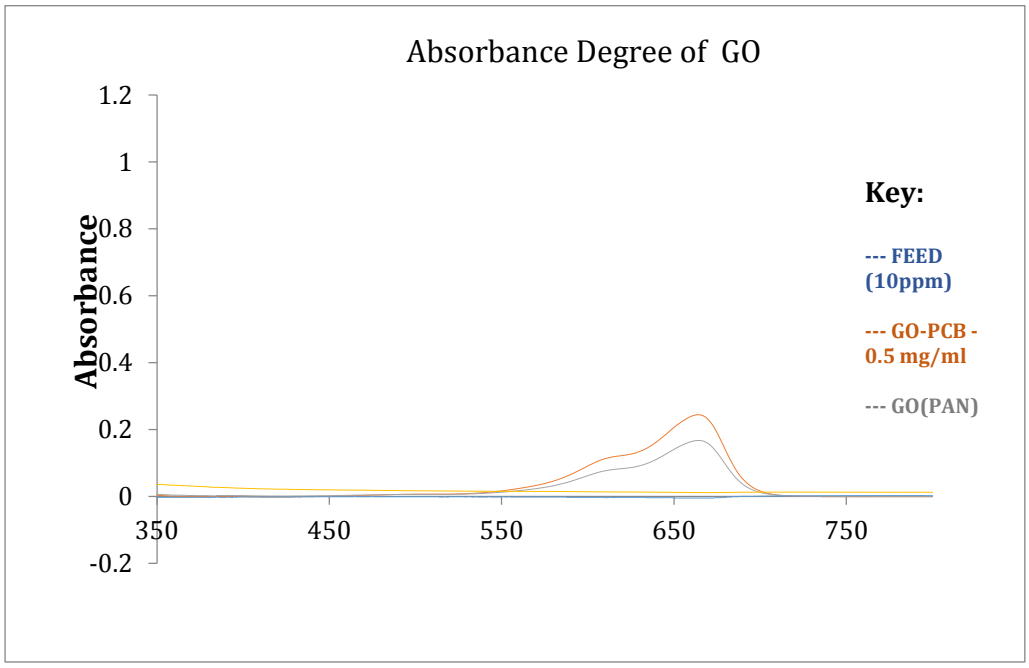

Figure A2 Absorbance Degree of Methylene Blue in GO Membrane at Higher concentrations